sustainability

MDPI

Article

Multi-Criteria Approach for the Study of Dam Silting Processes in Arid and Semi-Arid Regions: Example of the Assif El-Mal Watershed, Morocco

M'bark Abidare [1,*], Lahcen Daoudi [1], Ali Rhoujjati [1] and Nathalie Fagel [2]

[1] Laboratory of Georessources, Geoenvironment and Civil Engineering (L3G), Faculty of Sciences and Technology, Cadi Ayyad University, Marrakesh BP549, Morocco; l.daoudi@uca.ac.ma (L.D.); a.rhoujjati@uca.ac.ma (A.R.)
[2] Laboratoire Argiles, Géochimie et Environnements Sédimentaires (AGEs), Département de Géologie, Quartier Agora, Bâtiment B18, Université de Liège, B-4000 Liège, Belgium; nathalie.fagel@uliege.be
* Correspondence: m.abidare.ced@uca.ac.ma; Tel.: +212-637466514

Abstract

In arid and semi-arid regions, the hydro-sedimentary processes responsible for reservoir siltation remain insufficiently studied. This study focuses on the Taskourt Dam, one of the major reservoirs in the Marrakech-Safi region in central Morocco. A 450 cm thick sediment core was collected from the reservoir to assess the impact of extreme flood variability on sediment dynamic. A multi-approach analysis was conducted, including sequence analysis, grain-size and bulk and clay mineralogy of the sediments. In addition, hydrological parameters, instantaneous discharge, historical variations in daily water volumes in the reservoir, spillway discharge volumes, and siltation rates were determined through bathymetric surveys. The aim is to identify and evaluate the dynamics of sedimentation evolution within the reservoir. The results highlight two major phases in the siltation history of the Taskourt reservoir. (1) From 2011 to 2016, the siltation rate experienced rapid growth, marked by several major flood events. This intense sedimentary dynamic is illustrated by an accumulation of 418 cm of sediments. The floods of 2014 and 2016 strongly contributed to the intensification of flow energy and to a significant sediment load during this period. (2) From 2017 to 2023, the siltation significantly slowed down, associated with a prolonged drought period. This trend is recorded by a limited sedimentary deposit of 32 cm in thickness. This study provides valuable insights for the development of integrated sediment management strategies, supporting sustainable reservoir operation and effective planning, particularly in similar contexts worldwide.

Keywords: dam sedimentation; soil erosion; bathymetric survey; sedimentation couplets; watershed

Academic Editor: Liying Sun

Received: 31 December 2025
Revised: 5 February 2026
Accepted: 9 February 2026
Published: 13 February 2026

1. Introduction

Due to climate changes, rapid population growth, and the expansion of industrial, energy, and agricultural sectors over the past decades, global water demand has increased significantly. Various strategies have been adopted to mitigate this water scarcity, among which dam construction stands out as one of the most important, increasingly becoming a top priority [1]. In the 1960s and 1970s, the construction of large artificial reservoirs

peaked, with nearly 62,339 such dams currently existing worldwide. However, many of them have aged and are experiencing increased sedimentation [2].

In arid and semi-arid regions, sedimentation of these hydraulic structures represents a major and complex issue. Soil water erosion emerges as the primary process, of natural and/or anthropogenic origin, responsible for sediment accumulation in surface water storage areas [3]. Spatial assessment of erosion helps identify the main sediment-generating zones, contributing to a better understanding of the sources responsible for the siltation of these infrastructures [4]. The acceleration of this phenomenon poses a significant challenge for the sustainable management of land and water resources in many regions worldwide [5–7]. In the future, the risk of sedimentation in hydraulic infrastructures is expected to increase due to the combined effects of climate change and human activities, which promote soil degradation [7–9].

Every year, tens of tons of soil are eroded and transported directly to dams during flood periods. Understanding this phenomenon in arid and semi-arid regions, which record the highest erosion rates, is crucial due to the increasing scarcity of water, exacerbated by significant spatial disparities and temporal irregularities [10]. Soil degradation in watershed areas is a widespread phenomenon across most regions of the Maghreb, due to the convergence of conditions particularly favorable to its onset and progression. These include the low resistance of soils to erosion, climatic irregularities, sparse vegetation cover, the occurrence of violent floods, as well as anthropogenic pressures (deforestation, overgrazing, wildfires, poor agricultural practices, and urbanization) [11,12]. In Morocco, soil loss is the main factor contributing to reservoir siltation. These losses exceed 20 tons per hectare per year (t/ha/year) in the Rif region in the north, range between 10 and 20 t/ha/year in the Pre-Rif, and vary between 5 and 10 t/ha/year in the Middle and High Atlas [13]. The total annual sedimentation volume of reservoirs is estimated at 75 million cubic meters (Mm^3), representing more than 0.5% of their storage capacity per year [14,15].

Numerous studies have been conducted to better understand and provide detailed information on historical sediment dynamics in dam reservoirs. The indirect method, based on estimating sediment yield (SY) from the volume of sediments deposited in these reservoirs, serves as a valuable tool, particularly for validating sediment yield modeling approaches [16–20]. However, ref. [21] highlights several limitations of this method, including its accuracy in estimating sediment storage, the interpretation of historical sedimentation dynamics, and the fact that the calculated sediment yield represents an average over an extended period. Therefore, sediment coring and paleolimnological techniques are essential for gathering such detailed information [19,22]. Most researchers use sediment cores to establish an accurate chronology of sediment deposition associated with flood events, sediment transport, and deposition processes [19,20,23–26]. The analysis of these sediment cores makes it possible to clearly distinguish specific events, such as distinct couplets related to extreme flood events, and to estimate the sediment yields associated with them. However, current knowledge regarding the completeness of paleo-flood records, as well as the influence of discharge on the formation and thickness of flood deposits, remains limited [27]. In particular, few studies have examined these dynamics in the arid and semi-arid contexts of North Africa, where extreme hydrological conditions and flood variability strongly shape sedimentation processes in reservoirs. This scientific gap highlights the need for integrated studies that link hydrological dynamics with sedimentological and mineralogical characteristics. Our study adopts this innovative perspective by combining sedimentological, mineralogical, and hydrological approaches to reconstruct and interpret the sedimentary dynamics of dams, thereby providing an original contribution to the understanding of siltation processes in the arid and semi-arid environments in general, and in those of Morocco in particular.

Aligned with this objective, the present study aims to gain a better understanding of dam siltation processes in arid and semi-arid regions and to anticipate their impacts on the sustainability and functioning of such hydraulic structures. To this end, we focus on the Taskourt dam, which is currently experiencing a severe sedimentation problem due to the heightened risk of soil erosion in its watershed, particularly in the context of its recent construction. This watershed is characterized by high relief, diverse lithologies, sparse vegetation cover, and irregular rainfall patterns. Since the beginning of the construction of this dam, the Oued Assif El-Mal has become an important river to monitor in order to mitigate the effects of floods in the downstream part of the watershed, where the dam is located and which is heavily exploited. The sediment transport and deposition processes have shown considerable variability due to the fluctuating hydrological regime of the wadi. The sediments retained by the dam since its commissioning, which we accessed through a 450 cm thick core, may provide valuable information on sediment deposition processes, the evolution of soil erosion, and environmental changes within the upstream watershed. Given the lack of studies on this subject and the availability of important data such as instantaneous discharge records, historical variations in the daily water volumes of the reservoir, historical variations in flood spillway discharge volumes, as well as sedimentation rates determined from bathymetric surveys conducted by the Tensift Hydraulic Basin Agency (ABHT), we adopted a multi-criteria approach. This approach integrates bathymetric data, analysis of deposit thickness and stratigraphy, granulometric distribution of sediment particles, mineralogical variation analysis, and correlation with documented historical discharge events. Additionally, the RUSLE model was used as a support tool to better characterize erosion-prone areas, which represent the main sources of sediments.

2. Study Area

The upstream watershed of the Taskourt Dam is part of the larger Tensift basin, located in the western part of the High Atlas Mountains (Figure 1). The outlet of this watershed (Taskourt reservoir) is situated approximately 100 km south-west of the city of Marrakech. Elongated in shape, the basin covers an area of 424 km^2, with elevations ranging from 954 to 3596 m. It is characterized by a sparse hydrographic network and exhibits low and irregular surface runoff. The Taskourt Dam, commissioned in 2011, is primarily supplied by the Assif El-Mal tributary.

Geologically, this basin is largely part of the Hercynian basement of the High Atlas chain, characterized by the emplacement of granitoids, notably those of Jbel Tichka, which are associated with significant metamorphism. Towards the south, outcrops are dominated by schists and volcanic rocks of Cambro-Ordovician age, which are particularly resistant to erosion (Geological map of Marrakech; 1:500,000). In the northern part, especially around the dam site, softer and more erosion-prone Mesozoic formations dominate with marl, dolomitic limestone, red sandstone, gypsum, clay and conglomerates.

The region is characterized by a continental climate of semi-arid to arid type, with an average rainfall of approximately 700 mm per year. The climate is influenced by the presence of the High Atlas mountain range [28]. Vegetation cover within the basin is sparse, and the majority of the area appears to consist of bare soils. Leptosols are the predominant soil type; these are shallow soils that occupy much of the High and Middle Atlas regions, particularly in elevated areas, where they develop on hard and compact magmatic and metamorphic rocks or on limestone formations [13].

https://doi.org/10.3390/su18041953

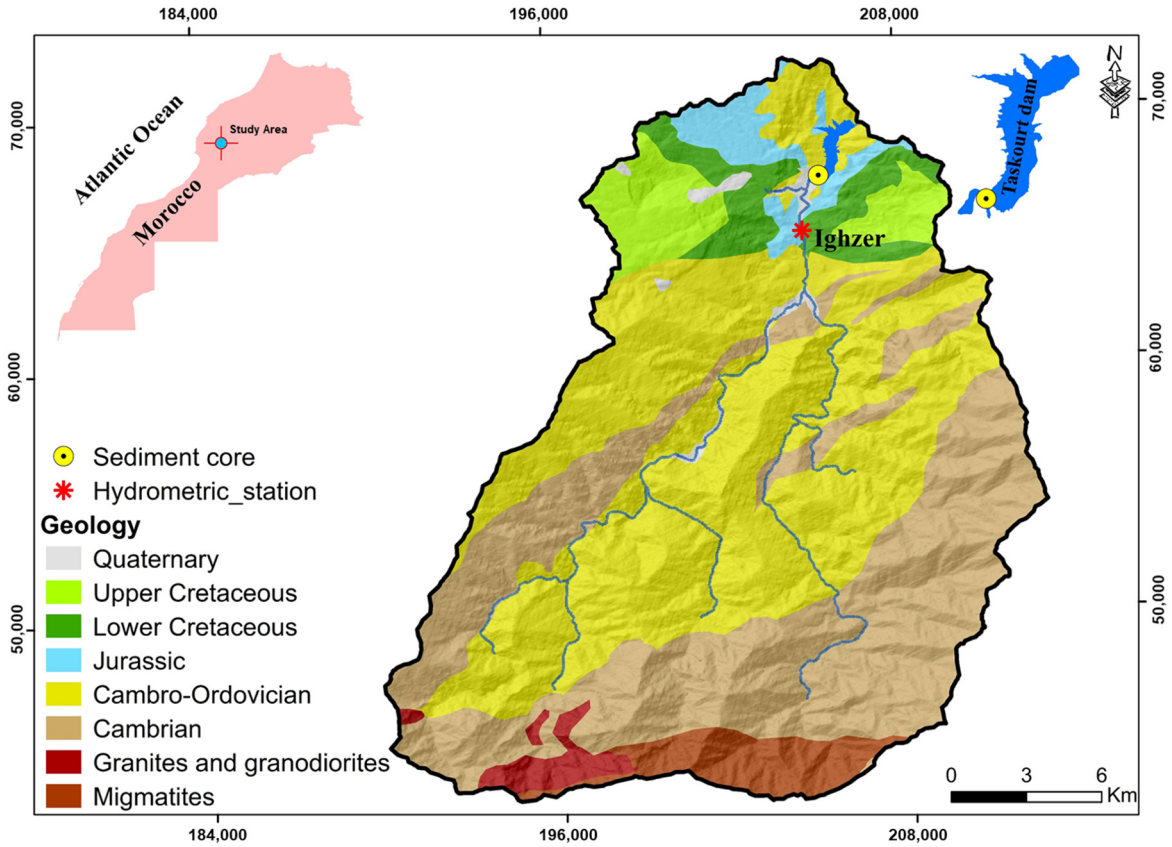

Figure 1. Geological map of the Assif El-Mal watershed.

3. Materials and Methods

3.1. Sampling

A 4.5 m sediment core was retrieved from the Taskourt Dam reservoir using a Russian corer (50 cm length, 5 cm diameter) during a coring campaign conducted in October 2023. This method offers the advantage of minimally disturbing the sedimentary sequences, particularly by avoiding compaction caused by the insertion of liners into the sediments. The core, composed of nine 50 cm sections, was extracted over a total thickness of 450 cm (Figure 2). The sampling site was carefully selected in the upstream zone of the reservoir, an area recognized as particularly favorable for recording variations in sediment inputs and hydro-sedimentary events [29]. The choice of this location is also justified by the organization of deposits within the sedimentary column. This position allows clear identification of repetitive sequences, each composed of fine-grained sands at the base, overlain by finer silt and clay layers at the top.

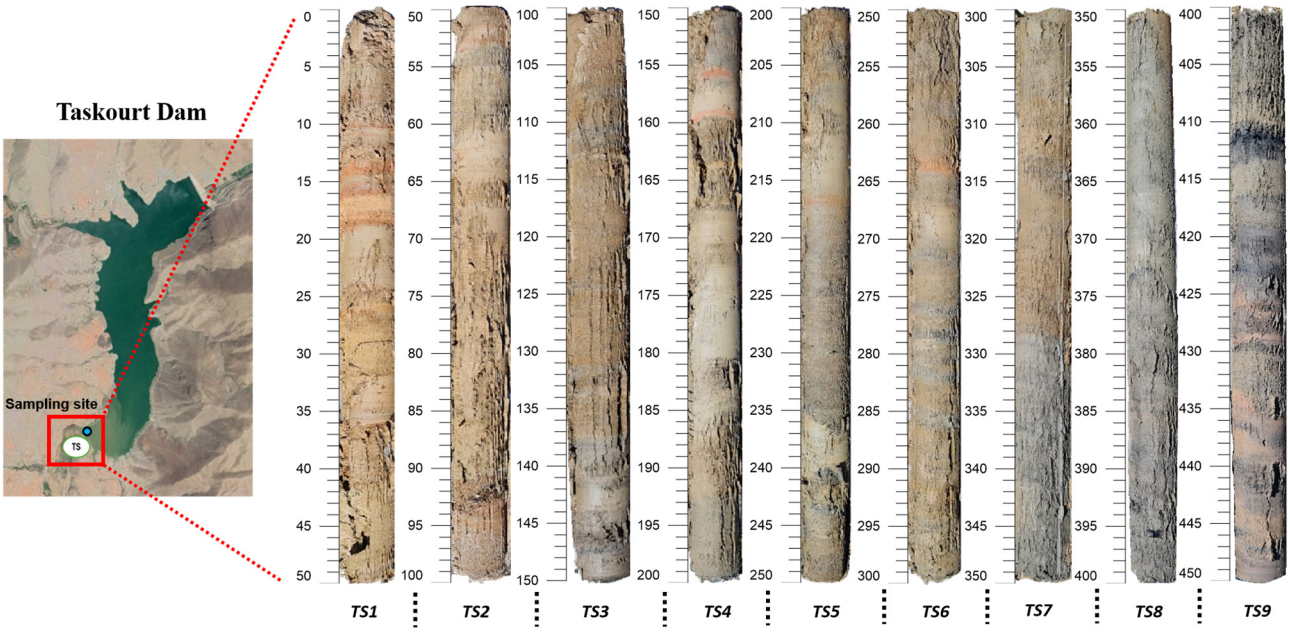

Figure 2. Photograph illustrating the lithological description of sediment core TS (TS1–TS9: Sections of 50 cm).

A macroscopic description of the sedimentary facies successions of the core was carried out. The succession of facies reveals an alternation between coarse and finer deposits, as well as between lighter and darker layers. The combination of these alternating patterns made it possible to identify 18 sedimentary sequences. The sedimentary evolution is used as a key criterion for selecting samples ($n = 74$) for more detailed analyses.

3.2. Analytical Techniques

The samples collected at various depths from the core were prepared for the analysis of grain size distribution, calcium carbonate and organic matter contents, as well as bulk and clay fraction mineralogy.

Grain size distribution was performed using a HORIBA LA-300 laser diffraction analyzer (size range 0.1–600 µm). This instrument operates on the principle of laser beam diffraction by particles suspended in a fluid, enabling detailed measurement of particle size distribution.

Calcium carbonate ($CaCO_3$) content of the samples was estimated using a Bernard calcimeter. Total organic matter content was measured through loss-on-ignition (LOI) method at 550 °C for four hours [30].

The bulk and clay fraction mineralogical compositions of the core samples were identified using X-ray diffraction (XRD), performed with a Bruker D8-Eco Advance diffractometer with a scan step size of 0.02° and time/step of 0.6 s equipped with a copper anode.

Bulk mineralogical analysis (powder form) was conducted following the procedure described by [31]. The relative mineral abundance was determined based on the height of the main peaks, using the correction coefficients adopted by [32].

For the analysis of the clay fraction, the bulk sediment was decarbonated using HCl (0.1 mol/L), and the <2 µm fraction was separated by decantation in a distilled water column. The samples were mounted as oriented aggregates on glass slides [33]. Three X-ray diffraction patterns were recorded successively: in the natural or air-dried state (N), after solvation with ethylene glycol for 24 h (EG), and after heating at 500 °C for 4 h (H). Clay minerals were identified and their percentages were estimated. Semi-quantitative analysis was performed taking into account the intensity of each peak and a specific correction factor for each clay mineral, following the approach described by [34].

3.3. Historical Hydrological Approach

In this study, we used bathymetric survey data collected in the Taskourt reservoir by the Tensift Hydraulic Basin Agency (ABHT). The available bathymetric survey series examined in this study date from 2013, 2016 and 2022. These datasets enable the determination of the sedimentation rate and its evolution within the reservoir, and to contribute to the chronological reconstruction of the sedimentary sequences.

Instantaneous water discharge data, recorded with a time resolution of four hours between 2009 and 2021, at the Ighzer hydrometric station, the nearest station to the reservoir, were also provided by ABHT. These data are used to explore potential correlations between water discharges and the sediment column of the core collected from the reservoir.

We also used other data, including variations in reservoir water volumes, filling rates, and floodwater discharged through the spillway. These data were obtained from the Ministry of Equipment and Water.

3.4. Normalized Difference Water Index

In this study, the detection of water mass information in the Taskourt reservoir was performed using the Normalized Difference Water Index (NDWI) on Landsat 7 and 8 satellite images (Equations (1)–(3)). This index enables the identification of water bodies by analyzing reflectance in the visible spectrum, particularly the green band, and the near-infrared (NIR) band [35,36]. High positive values (close to +1) typically characterize surface water, as water strongly reflects in the green band and absorbs in the NIR. Conversely, negative values or values close to zero indicate non-water surfaces (soil, vegetation) [37]. After detecting the water surface on Landsat 7 and 8 images, a supervised classification was performed using the Google Earth Engine (GEE) platform to refine the analysis and improve the accuracy of the results.

$$\mathrm{NDWI} = \frac{(\mathrm{Green} - \mathrm{NIR})}{(\mathrm{Green} + \mathrm{NIR})} \quad (1)$$

$$\mathrm{NDWI\_Landsat\ 8} = \frac{(\mathrm{Band3} - \mathrm{Band5})}{(\mathrm{Band3} + \mathrm{Band5})} \quad (2)$$

$$\mathrm{NDWI\_Landsat\ 7} = \frac{(\mathrm{Band2} - \mathrm{Band4})}{(\mathrm{Band2} + \mathrm{Band4})} \quad (3)$$

3.5. RUSLE Model

The RUSLE model was employed in this study to identify the spatial variations of critical erosion zones within the watershed, which represent the main sources of sediment input to the reservoir. The RUSLE model was selected because of its proven reliability, flexibility, and wide applicability in assessing soil erosion under various environmental conditions, including arid and semi-arid regions such as our study area. Compared with more complex physically based models, RUSLE requires fewer input parameters and readily available data, which makes it particularly suitable for data-scarce environments. In addition, its integration with remote sensing and GIS tools allows for efficient spatial representation and quantification of soil loss, as demonstrated in several recent studies [6,38,39]. Results validation was performed by comparing the erosion map with satellite imagery and field survey observations to confirm the correspondence between the mapped areas and the obtained results.

The quantification and identification of areas with potentially high soil erosion risk are carried out using the five factors expressed in the following equation [40,41]:

$$A = R \times LS \times C \times K \times P \quad (4)$$

where A represents the average annual soil loss in t/ha/year; R is the rainfall erosivity factor; K is the soil erodibility factor; L is the slope length factor; S is the slope steepness factor; C is the cover management factor; and P is the support practice factor.

The delineation of the watershed upstream of the studied dam, as well as the determination of the geomorphological parameters, slope length (L) and slope steepness (S), were based on the use of a Digital Elevation Model (DEM) with a spatial resolution of 30 m × 30 m, downloaded from the USGS Earth Explorer platform.

The soil erodibility factor was calculated using the formula presented by [42], based on the 2017 global soil map from ISRIC—World Soil Information, which provides data on soil properties including sand, silt, clay content, and organic carbon. These data were resampled at a 30 × 30 m spatial resolution.

The rainfall erosivity factor (R) used in this study was derived from the CHIRPS product with a spatial resolution of 0.05° × 0.05°. This product provides better accuracy for estimating the R factor at the watershed scale [43].

The cover management factor (C) was estimated using the Normalized Difference Vegetation Index (NDVI) derived from Landsat 8 imagery, by assigning a specific C-factor value to each vegetation type, following the approach proposed by [44].

The RUSLE model does not directly estimate sediment yield (SY), but provides an estimate of the gross erosion rate at the watershed scale. Therefore, the assessment of SY requires the integration of the Sediment Delivery Ratio (SDR), which quantifies the fraction of total erosion that is actually delivered to the watershed outlet. In this study, SY was estimated using the combined RUSLE/SDR approach, according to the relationship expressed in Equation (5). The results were then compared with the specific sediment yield (SSY) values calculated from actual data obtained from bathymetric measurements of the Taskourt Reservoir, using Equations (6) and (7), in order to evaluate the consistency and relevance of the estimates provided by the RUSLE model.

$$SY = E(RUSLE) \times SDR \quad (5)$$

E(RUSLE) represents gross erosion for the entire watershed, and SDR denotes the sediment delivery rate.

$$SSY = 100 \times \frac{SV \times dBD}{A \times TE \times T} \quad (6)$$

where SSY denotes the specific sediment yield (tons per hectare per year), SV represents the estimated sediment volume (m^3) derived from bathymetric measurements, and dBD is the dry bulk density of sediments (ton/m^3), estimated at 1.3 for Morocco [45]. A represents the total watershed area in hectares, T is the age of the reservoir (years), and TE denotes the trap efficiency, calculated according to Equation (7).

$$TE = 100\left(1 - \frac{1}{1 + 0.0021 \times D \times \frac{C}{A}}\right) \quad (7)$$

where D is a constant factor, ranging from 0.046 to 1, with an average value of 0.1 adopted for the case of Morocco [6]; C is the reservoir storage capacity (m^3); and A is the watershed area in km^2.

In predicting sediment yield (SY), we evaluated three of the most commonly used empirical methods, based on watershed area and the slope of the main drainage network [46–48]. Among these approaches, the most appropriate method for estimating the Sediment Delivery Ratio (SDR) was identified by comparing the estimated SY values [8]. In this study, the equation proposed by [47] was selected as the most relevant (Equation (8)).

$$SDR = 0.5656 \times (A)^{-0.11} \quad (8)$$

4. Results

4.1. Sedimentological Analysis

We present below the results of the various sedimentological analyses conducted on the sediment core samples. These include macroscopic description, grain size analysis, the evolution of calcium carbonate ($CaCO_3$) and organic matter (OM) contents, along with the mineralogical composition of both the bulk and the clay fractions (<2 microns).

4.1.1. Sediment Core Description

In terms of texture, the core sediments consist of repetitive sequences composed of very fine-grained sands at the base, overlain by layers of silt and clay at the top. Eighteen sequences with thicknesses ranging from 9 cm to 50 cm were identified. We also observed a correlation between sediment texture and color, coarser (fine sandy) sediments exhibit lighter colors, whereas finer (silty-clayey) sediments display darker colors.

4.1.2. Particle Size Analysis

Grain size analysis reveals significant variations with depth. The median grain size (D50) ranges from 9 to 134 μm. The coarsest sandy layers are observed at depths of 400, 230 and 100 cm. The percentage of sand measured along the core varies from 0.2% to 81%, with an average of 38%. The percentage of silt fluctuates between 13% and 77%, with an average of 47%. The percentage of clay varies from 5.8% to 33%, with a mean value of 15%. Grain size analysis results also allowed the identification of 18 sedimentary sequences (Figure 3). Each sequence consists of fine sand at the base, overlain by a layer of silt and then clay. The proportion of these three components (fine sand, silt, and clay) varies from one sequence to another.

4.1.3. Variations in $CaCO_3$ and OM

The calcium carbonate content ranges from 2% to 25%, with a standard deviation of 4.6%. The vertical profile shows certain fluctuations, the most significant of which occur at depths of 15, 262, and 434 cm, likely indicating increased input and accumulation of calcium carbonate at these levels.

Organic matter content ranges from 2% to 9%, with an average of 4.54% and a standard deviation of 1.7%. This variability suggests a certain heterogeneity in the vertical distribution of organic matter within the deposits.

In most of the analyzed sections of the sediment column, organic matter and calcium carbonate contents vary proportionally, as confirmed by the correlation analysis. Indeed, the Pearson correlation coefficient indicates a positive and statistically significant relationship between these two parameters ($r = 0.703$; $p < 0.001$). Both parameters show an inverse relationship with grain size; sediments with high levels of organic matter and calcium carbonate generally exhibit fine grain sizes (fraction smaller than 63 μm). This relationship is particularly pronounced in sequences 1, 8, and 18 (Figure 3).

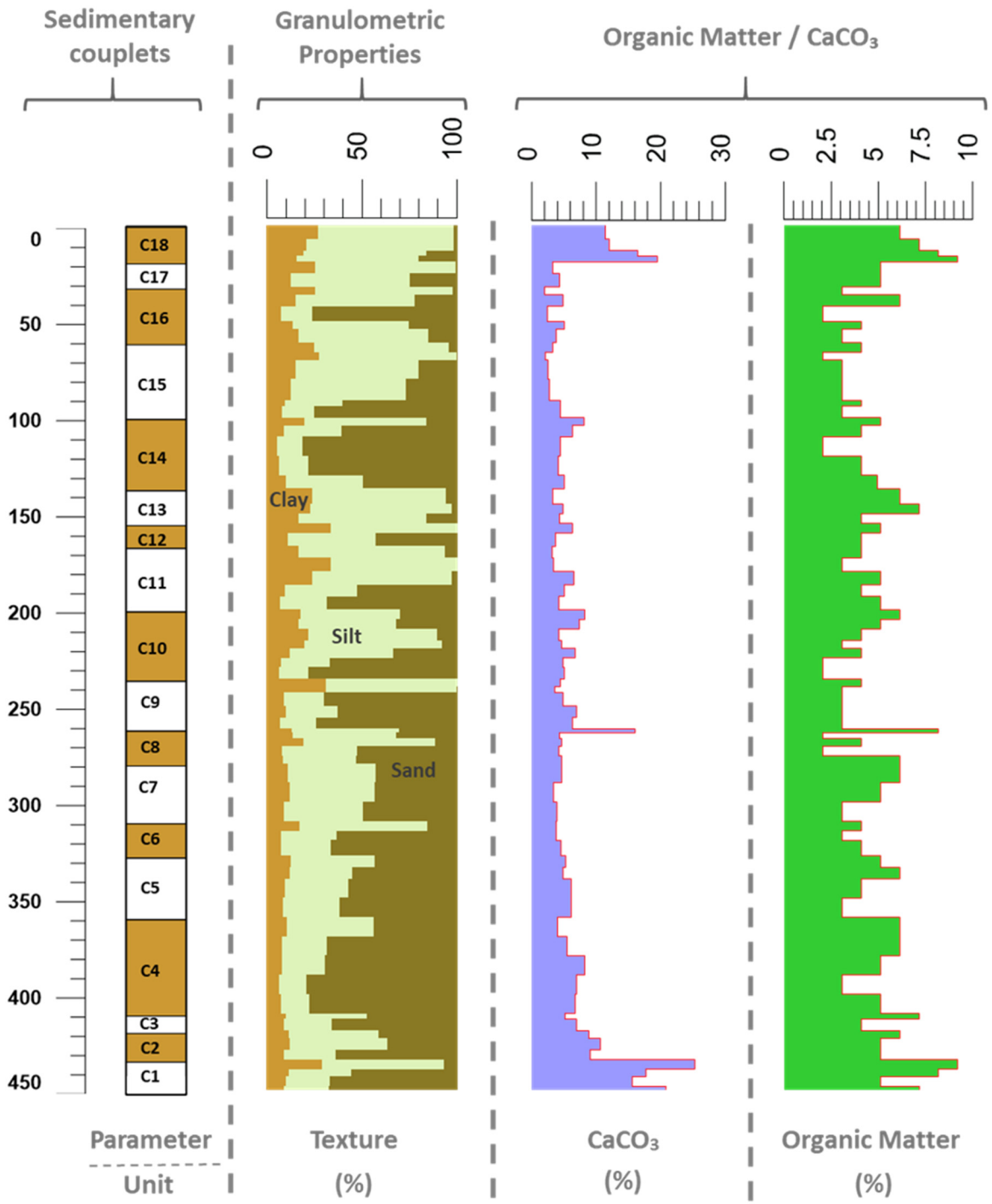

Figure 3. Vertical distribution of grain size, $CaCO_3$ content and organic matter along the TS sedimentary core.

4.1.4. Mineralogical Assemblage

X-ray diffraction analysis of the bulk mineralogy allowed the identification of the following main mineral phases: quartz (mean $\bar{x}$ = 33.15%; standard deviation σ = 5.77%), micas ($\bar{x}$ = 16.70%; σ = 5.03%), clay minerals ($\bar{x}$ = 14.14%; σ = 4.37%), dolomite ($\bar{x}$ = 10.51%; σ = 11.88%), plagioclase ($\bar{x}$ = 10.14%; σ = 2.75%), augite ($\bar{x}$ = 6.54%; σ = 1.45%), and calcite ($\bar{x}$ = 4.25%; σ = 2.75%). Other mineral phases, such as K-feldspars, hematite, and halite, are present in low abundance (Figure 4).

The contents of these minerals exhibit significant variability, being very low at certain depths while reaching relatively high values at others (Figure 5). Quartz is more abundant

in the sandy layers, whereas dolomite attains higher concentrations in sequences 1/2, 8/9, and 18, accompanied by a parallel increase in calcite. The two carbonate minerals show an opposite trend compared to the micas.

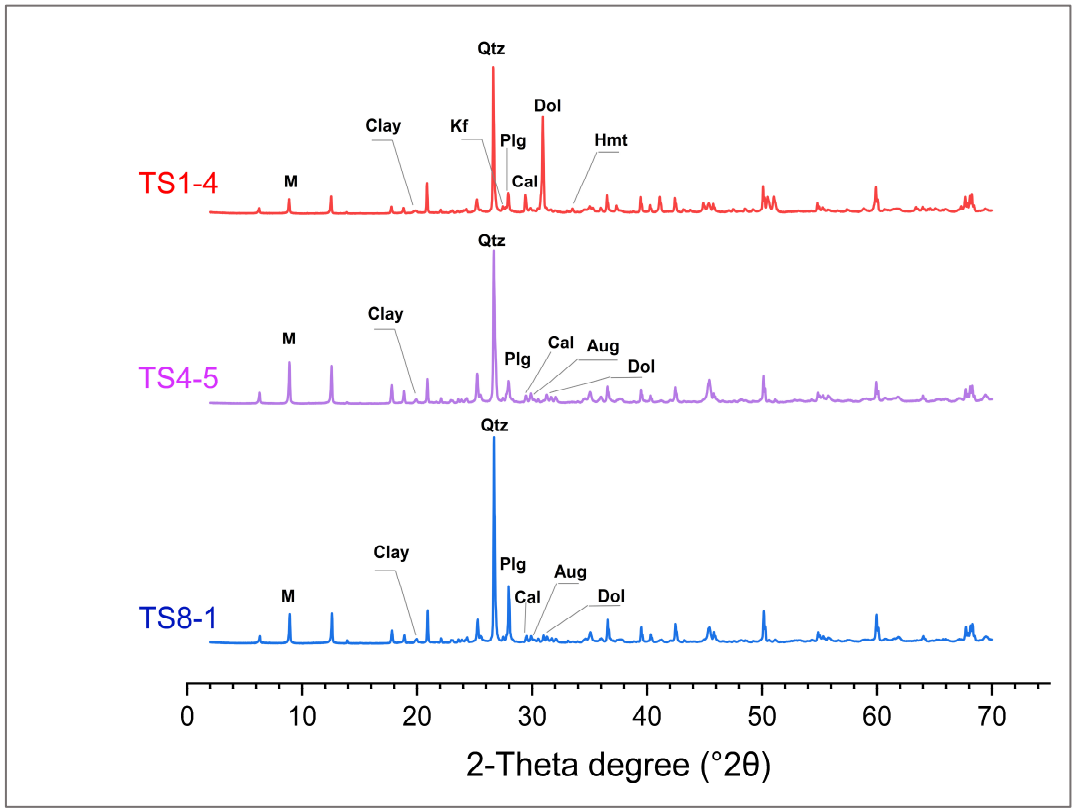

Figure 4. Example of X-ray diffraction (XRD) patterns of the bulk powder from three samples: TS1-4, TS4-5, and TS8-1. (Qtz: Quartz; Aug: Augite; Dol: Dolomite; Plg: Plagioclase; Cal: Calcite; Hmt: Hematite; Clay: Clay minerals; Kf: K-feldspar; M: Micas).

In the clay fraction (<2 μm), the identified clay minerals consist of, in order of relative abundance, illite (49 to 82%), kaolinite (11 to 39%), and minor amounts of chlorite and vermiculite (1 to 10%). Traces of smectite appear sporadically at certain depths (≤6%). Their presence coincides with sedimentary levels characterized by high carbonate concentrations, notably within sequences 1 and 18.

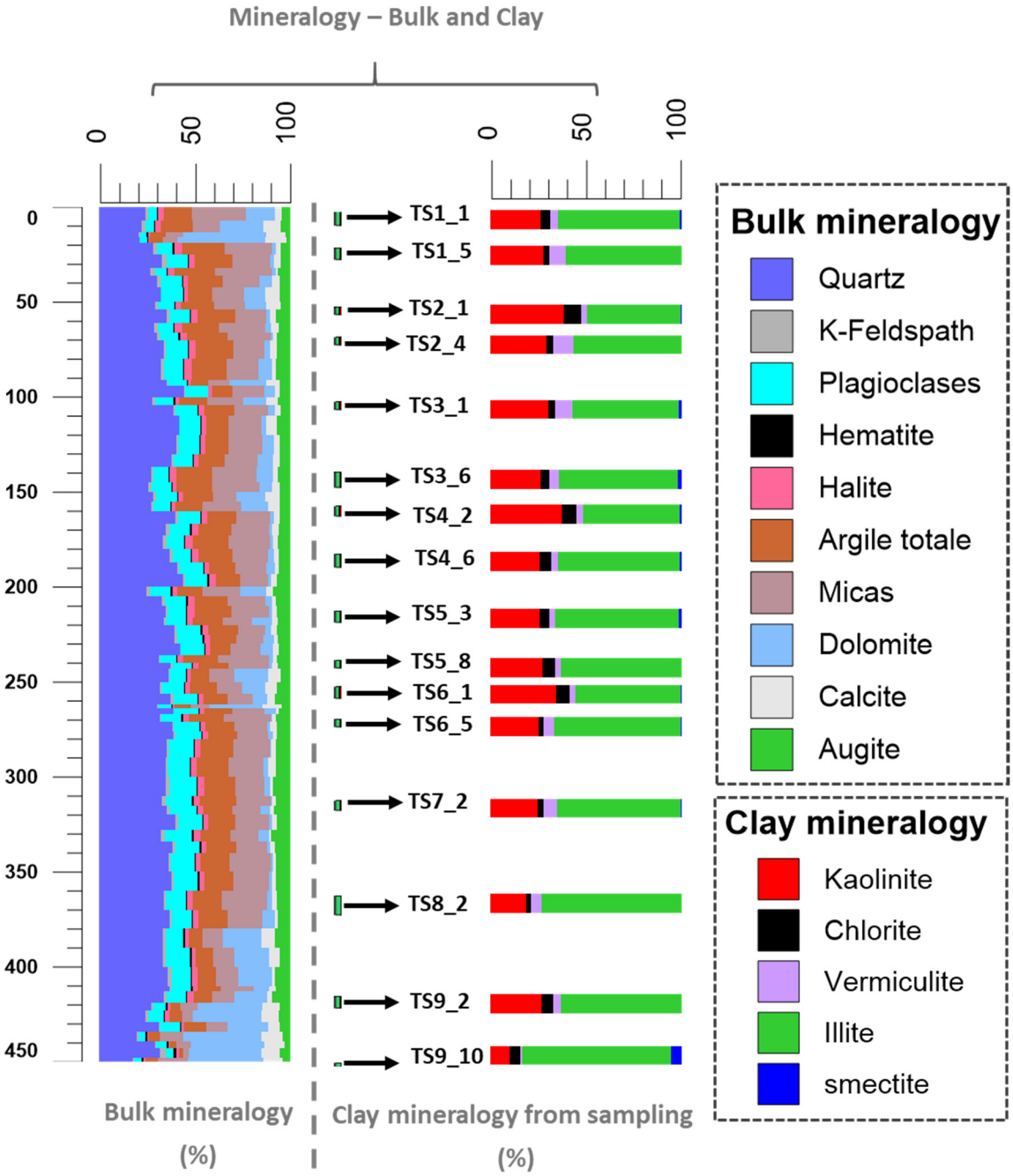

Figure 5. Vertical distribution of bulk mineralogy and clay minerals in the sedimentary core.

4.2. Hydrological Analysis

4.2.1. Bathymetry

Based on bathymetric surveys conducted in 2013, 2016, and 2022, it was possible to extract relevant information on the sedimentation rate in the reservoir and its evolution over time (Table 1).

Table 1. Sedimentation Data Based on Bathymetric Surveys.

Year	Period	Reservoir Volume at Normal Water Level (Mm^3)	Total Sedimentation Volume (Mm^3)	Cumulative Volume (Mm^3)	Sedimented Percentage (%)	Annual Sedimentation Rate (Mm^3/an)
2013		24.8				
2016	[2013–2016]	22.48	2.32	2.32	95.47	0.77
2022	[2016–2022]	22.37	0.11	2.43	4.53	0.017

Since the initial bathymetric survey conducted in 2013 at the Taskourt Dam, total sedimentation has amounted to approximately 2.43 Mm^3, representing a ≤ 10% loss of the initial storage capacity. This value is considered excessive compared to other dams in the region, especially given that the dam was only recently constructed. The normal capacity of the reservoir decreased from 24.8 Mm^3 in 2013 to 22.48 Mm^3 in 2016, representing a loss of 2.32 Mm^3, which accounts for 95.47% of the total sediment volume deposited. The loss was significantly lower between 2016 and 2022, with a reduction of only 0.11 Mm^3, corresponding to just 4.53% of the total accumulated deposits in the reservoir (Table 1).

The variation in sedimentation rate over this period highlights two distinct phases. The first phase is characterized by a high average sedimentation rate of 0.77 Mm^3/year between 2013 and 2016. The second phase is marked by a much lower rate of 0.017 Mm^3/year after 2016.

4.2.2. Variation in Instantaneous Water Discharge

In addition to the bathymetric analysis, instantaneous variations in water discharge recorded at the Ighzer hydrometric station, provide a second source of information used to establish a chronology of sedimentary sequences. This approach is based on the assumption that the identified sequences correspond to deposits resulting from the most significant flood events. To determine these floods, a threshold discharge is generally set, above which the flow is considered a flood event [49]. In the context of our study, the flood threshold is defined as a discharge equal to or greater than 10 m^3/s. Initially, this threshold was determined based on two main methods widely adopted for flood selection. The first, referred to as block maxima or annual maxima series (AMS) [50–52], is based on extracting the highest peak discharge recorded for each year from the available time series. Nevertheless, this method presents a major drawback: by considering only one event per year, it overlooks other extreme episodes that may occur during the same period, which can result in a significant loss of information regarding flood frequency, recurrence, and intensity. Moreover, in arid regions, some years may be marked by low or even nonexistent annual maxima. This affects the robustness of the analysis and may lead to the omission of several significant extreme events [50]. The second approach is referred to as the Partial Duration Series (PDS) or Peaks-Over-Threshold [49,53]. This method allows for the identification of several flood events occurring during a given period by defining an appropriate threshold, generally based on a chosen quantile corresponding to a relatively high non-exceedance probability, typically 95%, 99%, or 99.5% [49]. In this study, we adopted the peaks-over-threshold method by applying a 95th percentile, derived from instantaneous discharge data, to detect extreme flood occurrences within the basin. Subsequently, we prioritized a direct observational approach based on the analysis of instantaneous and daily discharge series in order to avoid prematurely limiting ourselves to strict theoretical considerations that could constrain the examination of natural phenomena in their actual form. This direct observation confirmed the initial relevance of the defined threshold, highlighting the selected value based on the available data.

4.2.3. Spatial Variability of Surface Water in the Reservoir

The analysis of instantaneous discharges and daily reservoir volumes reveals that no major flood events were recorded between 2016 and 2022, except one event in 2020. However, this flood was not sufficient to reach the full storage capacity of the reservoir (24.8 Mm^3). This situation suggests a limited hydrological dynamic, insufficient to flood the entire reservoir area, particularly the upstream zone. The latter, which includes the sediment core sampling site, remained dry during this period (Figures 6 and 7). In contrast, during the period from 2011 to 2018, as well as in 2023, the core sampling area was submerged by reservoir water, allowing for the successive recording of hydrological events within the sedimentary profile.

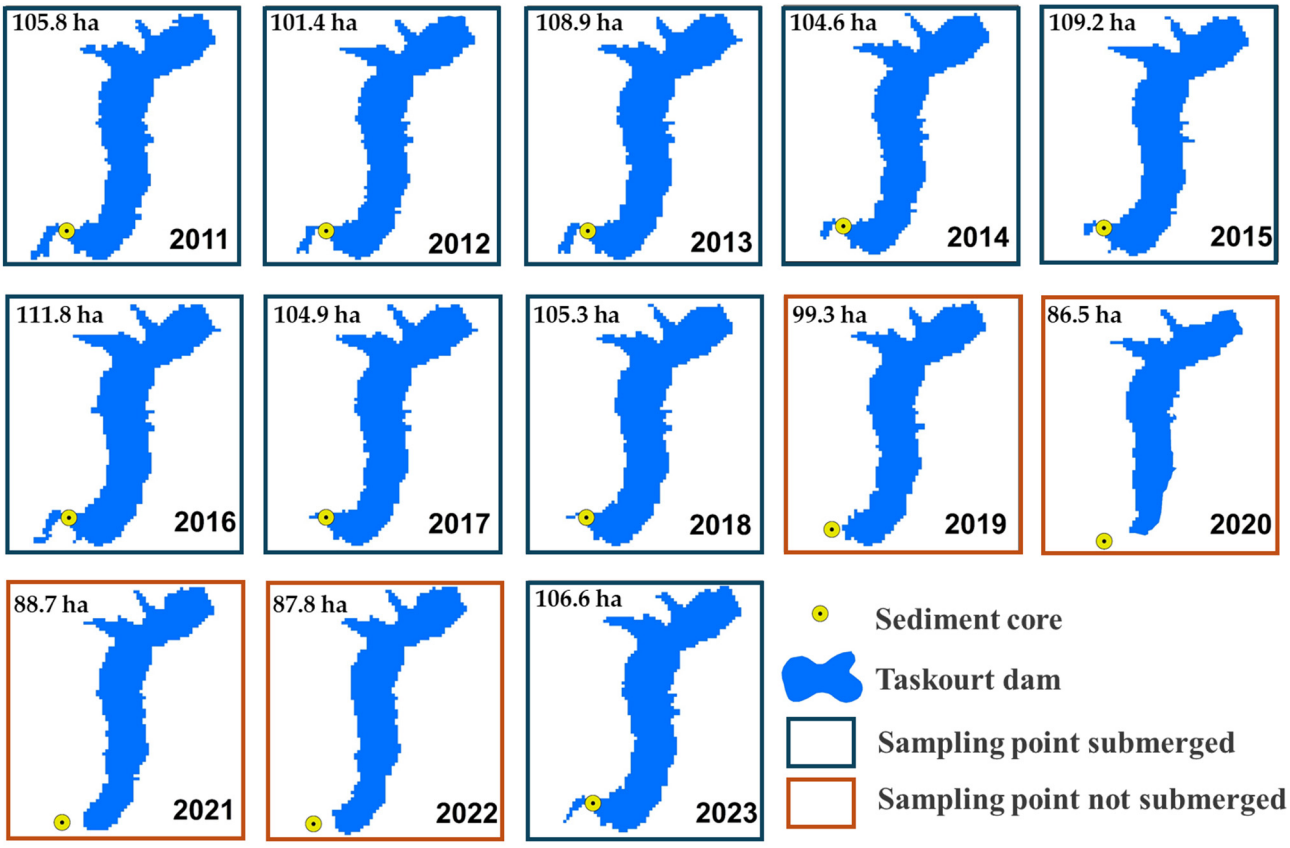

Figure 6. Variability of surface water in the Taskourt reservoir based on annual NDWI values, showing the location of the TS coring site relative to the water surface.

The variations in the water volume of the reservoir further confirm this situation (Figure 7). Since 2019, a prolonged drought has caused the stored water volume to remain more than 50% below the reservoir's original capacity. Although increases in volume were recorded in 2021 and 2022, the water level remained insufficient to inundate the core sampling site. However, at the time of core sampling in October 2023, the sampling area was located within the wetted zone of the reservoir.

Moreover, the normal storage capacity of the studied reservoir has been exceeded several times, as illustrated in Figure 7. This figure highlights that the spillway threshold was exceeded on multiple occasions, resulting in the discharge of water volumes through the flood spillway. The results indicate a strong relationship between discharges, water volumes, and the filling rate of the reservoir (Figure 7). High flow rates, particularly

during exceptional flood events, are strongly correlated with a significant increase in the water storage level of the dam.

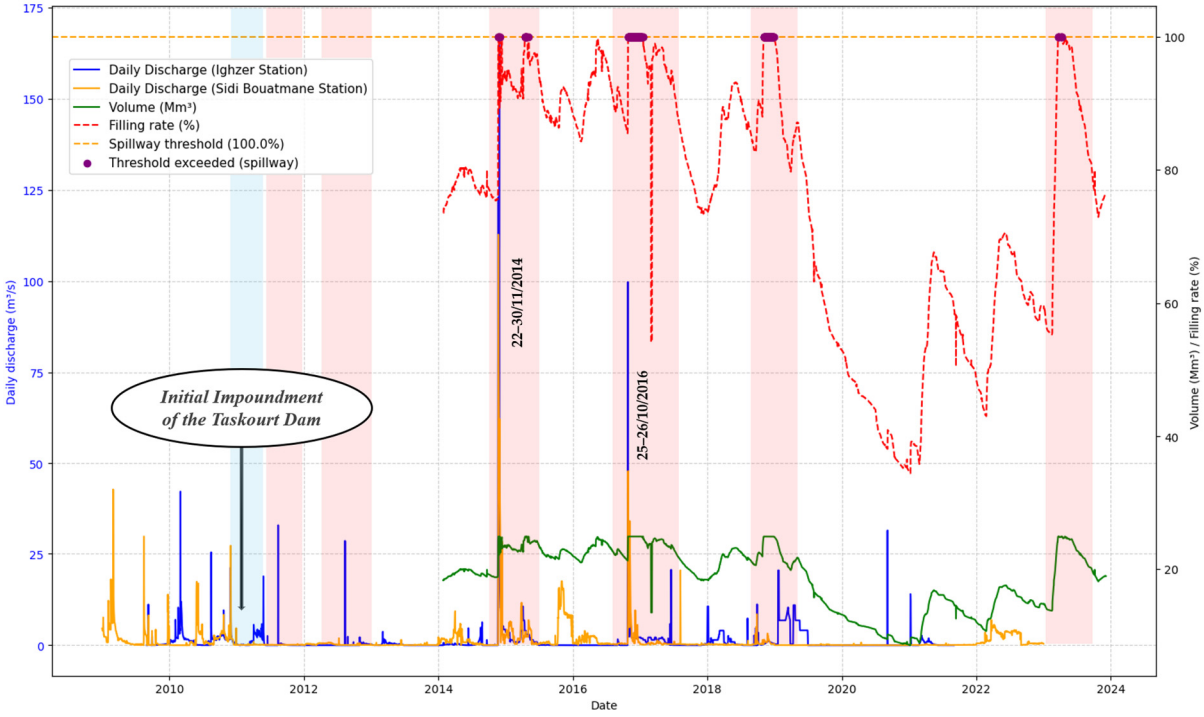

Figure 7. Daily variation in discharge and filling status of the Taskourt Dam (blue band: initial impoundment; red bands: recorded events).

Figure 7 also highlights the daily variations in discharge between 2009 and 2022, recorded at the Ighzer and Sidi Bouatmane stations, located upstream and downstream of the Taskourt dam, respectively. Following the beginning of reservoir impoundment in 2011, the discharge recorded at the Sidi Bouatmane station became lower than that measured at the Ighzer station, which can be explained by their relative positions with respect to the dam.

4.3. Analysis of Soil Erosion Risk

The multiplication of the maps generated for each factor [rainfall erosivity (R), soil erodibility (K), vegetation cover (C) and topography (LS)], highlights the spatial variations in potential soil erosion at the watershed scale with a 30 m resolution. We assigned a value of 1 for the P factor, due to the absence of significant conservation structures in the study area. This method was carried out in ArcGIS 10.8 using the Math Algebra tool. In our study, the LS factor plays a major role in capturing the combined influence of slope length and slope steepness on soil erosion processes. This factor is particularly relevant in our watershed, which is characterized by rugged topography and high slope variability. The analysis results indicate that areas exhibiting the highest erosion rates (>10 t/ha/year) are predominantly located on steep slopes subjected to intense precipitation, highlighting the amplifying effect of runoff energy. This spatial distribution confirms the predominant influence of topographic conditions, combined with climatic factors, in controlling water-induced soil erosion processes within the studied region.

In the Assif El-Mal watershed, the average soil loss risk is estimated at 30.4 t/ha/year. Approximately 84.9% of the watershed area experiences severe to very severe erosion (exceeding 10 t/ha/year), mainly affecting the southern zones characterized by sparse vegetation cover and steep slopes. Conversely, areas subjected to low to moderate erosion (less

than 10 t/ha/year) represent 15.1%, mostly located in the northern part of the watershed, where the terrain is gentler (Figure 8). RUSLE model outputs were validated through spatial consistency checks and comparison with known erosion-prone areas identified in field surveys, satellite observations, and previous studies [13,28]. Furthermore, a comparison between the sediment yield estimated by the RUSLE/SDR model and the value observed from bathymetric measurements revealed slight differences between the two approaches. In this watershed, the calculated SY is 8.84 t/ha/year, compared to an observed value of 8.94 t/ha/year. These differences remain small and confirm the reliability of the approach used to estimate sediment yield and the applicability of the RUSLE model for mapping erosion risk source areas. The difference between the estimated and observed sediment yield values is very low, at 0.10 t/ha/year, indicating that the model provides estimates consistent with the observations.

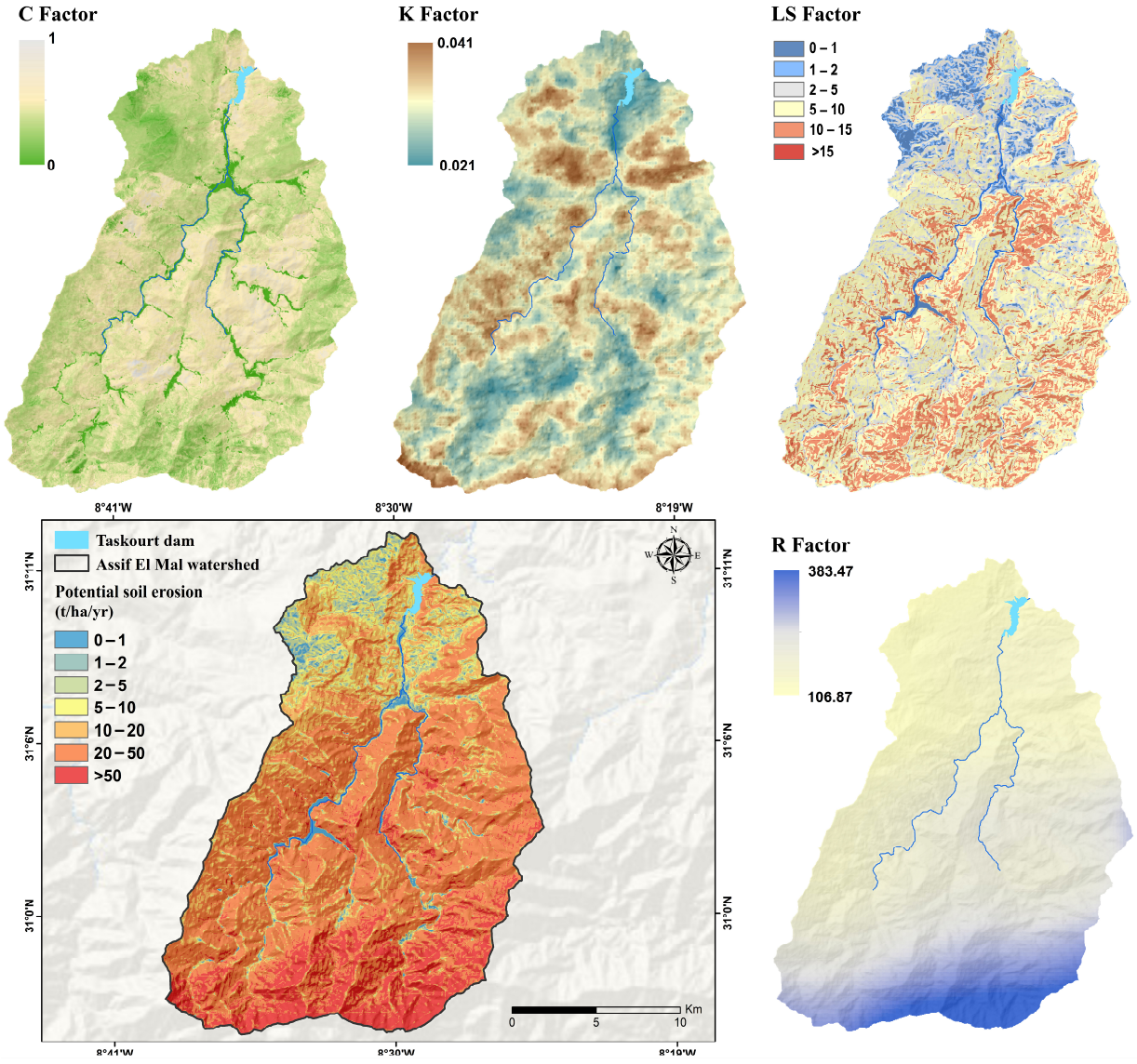

Figure 8. Soil erosion map of the Assif El-Mal watershed generated using the RUSLE model.

5. Discussion

In numerous studies, temporal variations in sediment load in dam reservoirs, as well as the identification of sediment sources and the main erosion mechanisms, have been assessed using mineralogical variations in accumulated sediments, based on analyses of bathymetric survey campaigns and instantaneous river flow measurements [19,20,26,54].

The novelty of this study lies in the analysis of sedimentation dynamics within a reservoir located in an arid zone, through an integrated approach combining hydrological and sedimentological parameters derived from cored sediments, aimed at reconstructing the temporal evolution of deposits.

5.1. Chronology of Sedimentary Sequences

In artificial reservoirs, cesium-137 (^{137}Cs) measurements have been widely used to establish sediment chronologies. This method is based on the assumption that this radioisotope is rapidly fixed in sediments after deposition, with no significant post-depositional mobility [24,55]. On a global scale, available data indicate that the maximum fallout of ^{137}Cs occurred between 1955 and 1966 [55]. In the case of the Assif El-Mal watershed, atmospheric fallout of radionuclides remained low and relatively stable throughout the operational period of the dam, and no major event could be identified as a chronological marker for dating the sediment deposits. This method could not be applied in our case study.

Based on a multi-criteria approach integrating bathymetric data, analysis of the thickness and organization of deposits, grain size distribution of sediment particles, mineralogical variation analysis, as well as the correlation with documented historical discharge events, we established a chronology of the couplets within the sediment core column.

5.1.1. Contribution of Bathymetry

Bathymetric analysis stands out as a particularly relevant indirect dating method for reconstructing the chronology of sediment deposits associated with flood events [19]. In the context of this study, this approach revealed that, from the initial bathymetric survey conducted in 2013 to the latest survey carried out in 2022, nearly all sedimentation, estimated at 95.47% of the total deposited sediment volume, occurred during the period 2013–2016. This intense sedimentary dynamic coincides with the two major flood events that occurred in 2014 and 2016, whose significant impact on sediment mobilization and transport is confirmed by the stratigraphic analysis of the core sample. In contrast, the period after 2016 accounts for only 4.53% of the total accumulated deposits within the reservoir, reflecting a marked decrease in sediment flux during this phase. The variations in sediment supply and the siltation rate of the dam reservoir are influenced by climatic conditions, which determine the frequency and intensity of floods, key factors in sediment mobilization and transport [19,55,56].

The sediments accumulated in dam reservoirs represent a direct archive of sediment production from the upstream watershed since the commissioning of the structure, both in the short term (on the scale of hydrological events) and in the long term [21]. Based on this approach, we were able to highlight valuable information, suggesting that sedimentary activity was more intense during the first phase, between 2013 and the end of 2016. In contrast, the second period, post-2016, is characterized by a drop in sedimentation.

5.1.2. Contribution of the Hydrological Approach

The chronological identification of sediment layers associated with flood events, based on the core extracted from the Taskourt dam, provides a relevant basis for analyzing past hydro-sedimentary dynamics and their impact on the increasing siltation of the reservoir.

In this study, the sediment layers were first identified and characterized based on objective criteria, such as grain size, thickness, and internal organization of the deposits, independently of hydrological data. The dating of the sedimentary couplets was then assigned using three complementary criteria: (1) the relative arrangement of the layers since the commissioning of the dam in 2011, (2) the sedimentological properties reflecting the

intensity of depositional events, particularly coarser and thicker deposits produced by floods with high sediment yield, and (3) the position of the core sampling site relative to the water surface, which helps confirm that these hydrological events were effectively recorded in the sedimentary archive. This approach ensures that dating is primarily based on sedimentological analysis, while hydrological data provide complementary context for interpreting the sediment regime and deposition chronology.

The sedimentary profile highlights 18 sedimentary couplets that correspond to flood events in the Assif El-Mal watershed (Figure 9). Among these layers, those associated with the extreme storm events of 2014 and 2016 [57] served as key chronological markers for establishing the chronology of the sedimentary couplets. These floods deposited particularly thick sediment layers with coarse grain sizes, marked by a significant increase in D50 values, especially for couplets C4, C10, and C15.

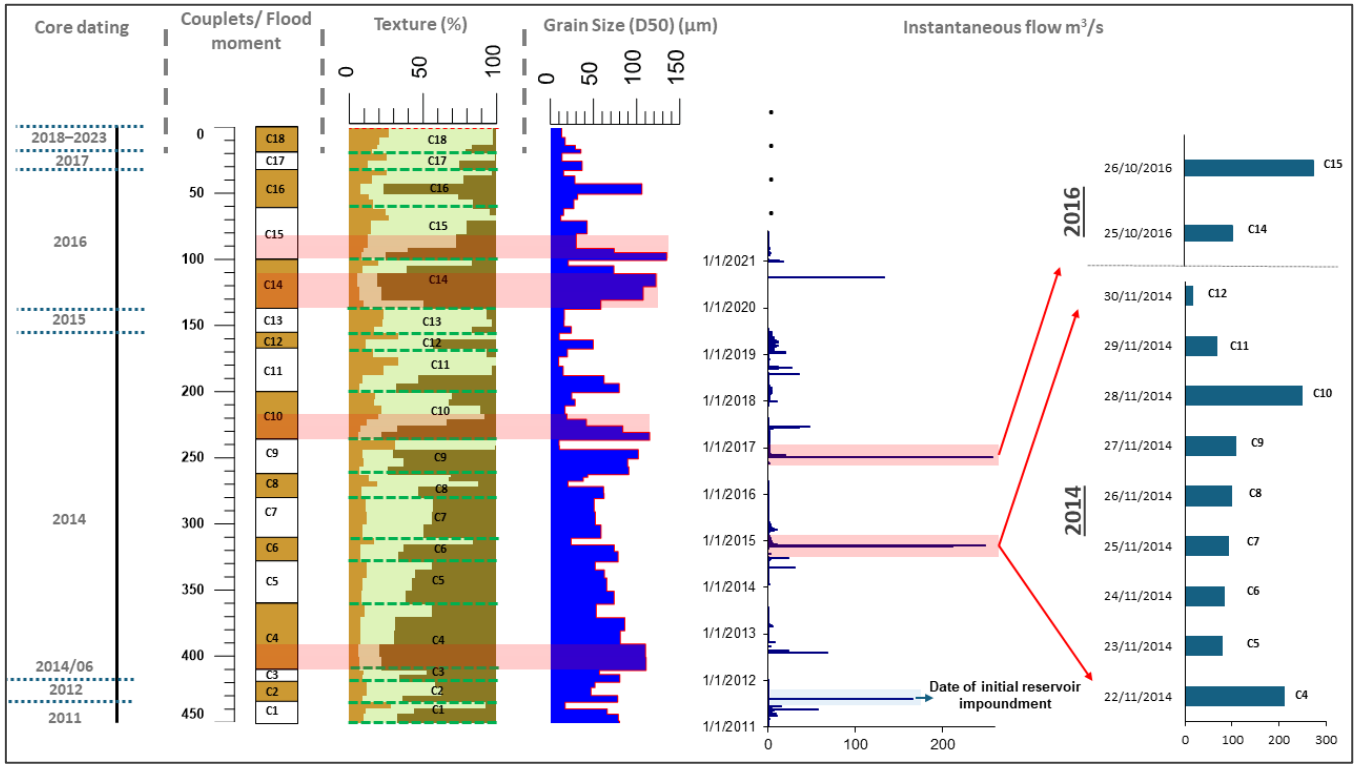

Figure 9. TS sediment core and corresponding instantaneous discharge (blue band: initial impoundment; red bands: major events).

The 2014 and 2016 flood events, which had significant economic, social, and environmental impacts in the Tensift basin [57], contributed to the dramatic sedimentation rate observed in this study. The year 2014 was marked by severe flooding, particularly during the weekend of 22 November. These events triggered sudden flash floods that resulted in the deaths of 36 people, primarily in the Guelmim region [49,58]. The coarser and lighter-colored layers, observed between 32 and 450 cm depth, could be associated with major flood events accompanied by massive sediment transport.

The lower sequence (C4) corresponds to the thickest sedimentary deposit in the profile, resulting from a substantial accumulation of coarse materials, likely deposited during the flood of 22 November 2014 (Figure 9). This intense event resulted in a 50 cm thick deposit, reflecting the strong sedimentary dynamics. This sediment layer thus represents a major chronological marker for interpreting the profile, due to its direct association with a significant flood event during that period. A second flood event, even more intense according to the flood records from the Ighzer hydrometric station, occurred on 28

November 2014. It also resulted in the deposition of coarse sands, clearly identified in sequence C10. Finally, the flood that occurred between 25 and 26 September 2016 is responsible for the deposits observed in sequences C14 and C15.

The interval between couplets C4 and C12 exhibits an alternation of sand-dominated granulometric levels, reflecting a fluctuating sedimentary dynamic characterized overall by high energy. This internal structuring suggests deposition in multiple successive pulses, likely linked to the instantaneous peak discharges recorded between 22 and 30 November 2014, during the major flood event. The dominance of sand confirms the prevalence of high-energy hydraulic conditions throughout this event. These likely correspond to long-duration floods caused by persistent storm episodes. Consequently, sub-daily discharge data are essential for analyzing short-duration hydrological events with high erosive and sediment transport potential, which are often overlooked or underestimated by daily averages. The importance of such data has been clearly demonstrated by [59].

5.2. Impact of Soil Vulnerability on Sediment Supply

In arid regions, the soil surface layer is rarely saturated with water, unlike in humid areas where soil saturation is a common condition. Indeed, infiltration-excess runoff is the dominant process during rainfall periods due to sparse vegetation and low air humidity, whereas in humid zones, saturation-excess runoff predominates [49]. At the end of the wet season, the concentration of suspended sediments tends to decrease due to dilution effects and less availability of erodible material [60]. In these regions, especially mountainous areas, natural hazards such as intense rainfall and flash floods exacerbate erosion processes and significantly contribute to soil degradation [61,62]. Furthermore, soil degradation accelerates when heavy rains fall on dry soil, following intensive land disturbance caused by agricultural activities.

The increase in flood events in the Assif El-Mal watershed, along with the water inflows to the Taskourt reservoir between the year the dam was commissioned and the end of 2016, reflects a period of intensified runoff at the regional scale. This trend was particularly marked by episodes of heavy rainfall recorded in 2014 and 2016, which triggered high-level flood alerts in several southern regions of the Kingdom [49,57,58,63,64]. In contrast, a marked decrease in runoff is perceptible during dry periods, particularly from 2019 onward, as evidenced by the hydrological regimes recorded at the Ighzer station. Variations in discharge and flood frequency appear to be key factors influencing the spatio-temporal fluctuations in the sedimentation rate within the reservoir [20].

Numerous studies have highlighted the link between flood risks, high-flow events, and soil degradation [4,26]. The highest sedimentation rates coincide with periods of increased discharge, indicating intensified hydro-sedimentary dynamics that enhance the transport and deposition of suspended particles [65].

The application of predictive models to estimate soil erosion is particularly important, especially in watersheds where outlets are regulated by hydraulic structures (dams, lakes, etc.). In this study, the RUSLE model was used to identify areas with a high risk of water erosion. Its application also provides complementary information regarding the origin of sediments, thereby enriching the results obtained from the mineralogical analysis of sediments deposited in the reservoir. The results show that most of the upstream watershed presents a high risk of erosion, mainly in areas characterized by the presence of relatively soft schist formations, steep slopes, and sparse vegetation cover, conditions particularly conducive to accelerated soil loss. This dynamic is supported by mineralogical analysis, which reveals high mica contents throughout most of the profile, indicating significant weathering of the schist bedrock and, consequently, a higher soil susceptibility to erosion. However, a decrease in mica content accompanied by an increase in carbonates is observed in certain parts of the profile. This trend could be related to the

spatial distribution of precipitation around the reservoir, where carbonate geological formations predominate. This observation is discussed in the section dedicated to mineralogy.

5.3. Relationship Between Discharges and Sedimentation Patterns

The analysis of the relationship between instantaneous discharges and sedimentation is essential for understanding hydro-sedimentary processes in reservoirs [65] (Table 2). The rhythmicity in sedimentary deposits reflects transport and deposition processes modulated by discharge fluctuations. Each couplet serves as an informative marker of flood-related deposition events.

Several studies highlighted the relationship between flood events and the intensification of erosion and sediment transport processes [19]. During storm events, sediment peaks and floods occur simultaneously, with larger sediment volumes recorded in response to higher discharges [55,65].

Sediment accumulations in reservoirs triggered by flood events often exhibit a characteristic vertical organization: a basal sequence with coarsening-upward grain size, corresponding to the rising limb of the flood, followed by a fining-upward sequence during the recession phase. However, the lower layers may be partially eroded or poorly preserved due to turbulence associated with peak discharge phases [25,60].

Table 2. Identified couplets and corresponding instantaneous flow (NA: no data available for 2023).

Events	Inst. Max. Flow (m^3/s)	Sedimentary Organization		Couplet Thickness (cm)	Couplets
		Sand Thickness (cm)	Silt–Clay Thickness (cm)		
2018–2023	36–(NA)	6	13	19	C18
18/06/2017	48.3	7	6	13	C17
05/11/2016	20	25	4	29	C16
26/10/2016	258	9	30	39	**C15**
25/10/2016	94.8	33	4	37	C14
06/04/2015	10.6	5	13	18	C13
30/11/2014	18.4	7	5	12	C12
29/11/2014	69.2	13	20	33	C11
28/11/2014	250	16	20	36	**C10**
27/11/2014	109.7	19	7	26	C9
26/11/2014	100.9	9	9	18	C8
25/11/2014	92.8	10	20	30	C7
24/11/2014	85.3	13	5	18	C6
23/11/2014	80.7	26	6	32	C5
22/11/2014	212.5	40	10	50	**C4**
30/06/2014	30.8	6	3	9	C3
12/08/2012	68.2	5	10	15	C2
15/08/2011	166.6	11	5	16	C1

In this study, we analyze the relationship between the maximum instantaneous discharge and the thickness of the sedimentary sequences observed in the TS core. Figure 10 highlights this correlation, as well as the relationships with the thickness of sands and silts/clays within each couplet. A moderate to strong positive correlation (R = 0.64) was observed between the maximum instantaneous discharge and the thickness of the sedimentary couplets. Such a strong correlation has also been reported in the literature [18–20,26]. It should also be noted that sediment deposits may undergo progressive

compaction over time, particularly under the effect of overburden, especially for sediments deposited over the long term. Consequently, the current thickness of the layers may be slightly less than their original thickness at the time of deposition. This phenomenon is common in lacustrine environments and reservoirs, and should therefore be taken into account when interpreting sedimentary records [66]. In this study, the effects of compaction were considered negligible, as the sediments examined are relatively recent (the oldest core samples date back to 2011).

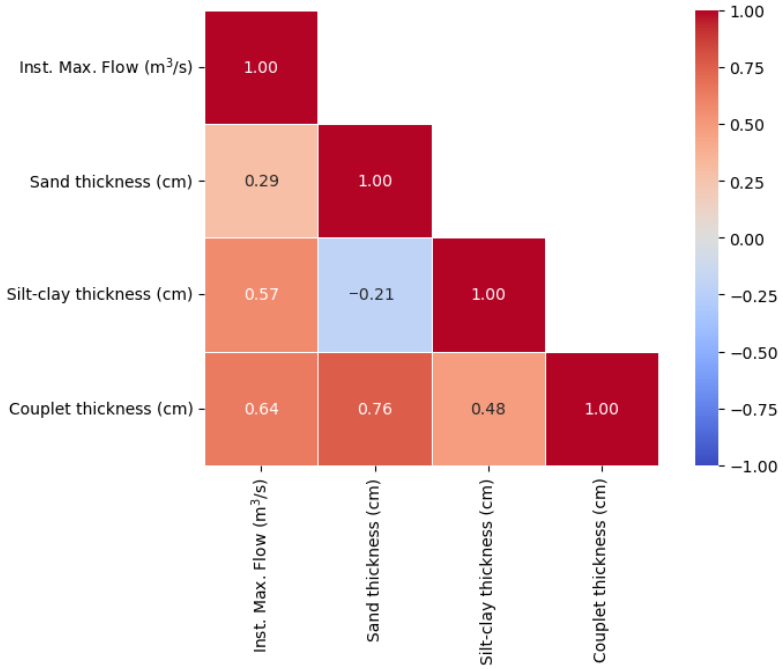

Figure 10. Correlation between instantaneous maximum discharge and sediment thickness in the TS core.

Increases in discharge within the watershed can intensify erosion processes, resulting in a rise in suspended sediment concentration. Moreover, high water stages enhance bank erosion, locally causing collapses. These collapses rapidly supply the watercourse with loose sediments, which are then transported as diluted sediment flows. These transient inputs contribute to the transport and potentially to the deposition of materials within the riverbed or in calmer settling zones downstream [60].

5.4. Contribution of Mineralogy

The nature and mineralogical variations contained in sedimentary deposits in accumulation environments depend both on physical depositional processes and post-depositional chemical processes [19,67]. In the studied reservoir, the amount of organic matter and carbonate contained in the sediments is low, with no significant impact on the interaction process with clay minerals. Moreover, the residence time is relatively short to allow for the transformation of clays [19]. In this context, the composition and evolution of the different clay assemblages in the sediment deposits of the investigated reservoir mainly reflect the physical processes of erosion, sediment transfer, and deposition, rather than in situ transformations and post- depositional chemical processes.

The variability in the mineralogical composition of the core samples reflects the variability of the geological formations outcropping in the Assif El-Mal watershed. The different geological units range from the Cambrian to the Cretaceous, with schist being the dominant geological facies in the upper part of the basin. In the downstream area, around

the dam, softer sedimentary rocks outcrop, composed of limestone, dolomites, and more or less weathered marl rocks.

The relative variations in micas and carbonates (calcite and dolomite) may be related to the spatial distribution of precipitation (Figure 5). The increase in carbonate mineral content suggests heavy rainfall in the lower part of the watershed, mainly composed of carbonate rocks (limestone and dolomite). This observation is supported by the local occurrence of low smectite contents at certain depths, particularly in areas with the highest carbonate percentages, which reflects irregular rainfall patterns typical of semi-arid regions. Smectite is primarily identified in the clayey fraction of soils developed on carbonate outcrops of the Lower Jurassic and Upper Cretaceous in the downstream area of the watershed [19,68]. Conversely, the increase in mica/illite content rather indicates a concentration of precipitation and intense erosive processes in the upstream area of the basin, mainly composed of schists. The mineralogy of the clay assemblages accumulated in the Taskourt reservoir during a given rainfall event represents the properties of the soils impacted by the corresponding precipitation.

The clay assemblage detected within the <2 μm size fraction of the core sediments is less diverse, mainly composed of illite and kaolinite with low abundance of chlorite, vermiculite and smectite (Figure 5). The relative abundance of illite is explained by the highest concentration in the clay fraction of the sedimentary formations from the Paleozoic to the Quaternary in the Western High Atlas basin [4,68]. A study conducted by [19] in the N'fis watershed, which exhibits climatic, topographic, pedological, and lithological conditions similar to our study area, also shows that illite is the predominant clay mineral phase in the sediments.

In terms of organic matter and calcium carbonate content, there is a correlation with the grain size of the deposits; most sediments with high carbonate and organic matter content are generally characterized by fine grain size (fraction less than 63 μm). The abundance of carbonates and organic matter in sedimentary layers can be explained by the flocculation of fine particles [69,70]. The deposits accumulated in the downstream part of the reservoir are finer, predominantly silty-clayey or clayey-silty, and exhibit a relatively high degree of flocculation [71,72].

5.5. Limitations and Implications for Management

The sedimentary dynamics of the Taskourt reservoir reveal distinct phases associated with variations in extreme flood events. This pattern is consistent with observations from other recent studies on sediment cores documenting hydrosedimentary responses [19,24,73]. Our study uniquely provides a continuous sediment record from 2011 to 2023, highlighting abrupt changes in sedimentation linked to major floods and prolonged droughts. Overall, the multi-criteria approach adopted, integrating hydrological, sedimentological, and mineralogical analyses, represents a novel and integrative framework for diagnosing sediment dynamics in reservoirs, particularly in arid and semi-arid catchments. This approach not only enhances our understanding of sediment accumulation processes but also offers valuable insights for reservoir management and predictive assessment, demonstrating the scientific contribution and originality of the work.

Despite these contributions, the study presents certain limitations. Due to the relatively high filling rate of the reservoir, field access was restricted, which prevented the collection of additional sediment cores from internal sections of the reservoir. Consequently, reliance on a single sediment core may not fully capture the spatial variability of sedimentation. In addition, during periods when the sampling site was not submerged, the sedimentary record of suspended inputs may be weak or absent, leading to local discontinuities in the stratigraphic sequence. However, these limitations do not contradict the main objectives of the study, which focus on understanding the dominant

sedimentation processes and their temporal evolution within the reservoir, rather than on a detailed assessment of spatial heterogeneity. They do not undermine the overall validity of the conclusions; instead, they provide a transparent framework for interpreting the results and highlight directions for future research, notably through the collection of additional sediment cores to better constrain spatial variability. Furthermore, the RUSLE model could be extended to prospective applications by coupling it with future climate scenarios, including projected changes in precipitation and long-term land use and land cover (LULC). When combined with the Sediment Delivery Ratio (SDR), this framework would enable the estimation of future sediment yield and support long-term reservoir management and planning strategies.

Although our study focuses on reconstructing sedimentation dynamics from sedimentary records, it provides insights for integrated sedimentation management strategies. These strategies include preventive measures, such as holistic watershed management (vegetation restoration, construction of small retention structures to reduce sediment transport, sustainable agricultural practices), as well as the identification and prioritization of areas particularly susceptible to water erosion for protection, as they represent the main sources contributing to reservoir sedimentation. Curative interventions, such as periodic dredging of reservoirs, can also be implemented and adapted in this context, although they remain challenging due to their high cost. These practical recommendations, while dependent on available resources and local conditions, provide a framework to support management decisions aimed at reducing sedimentation and enhancing the sustainability of hydraulic infrastructures in the region and in similar contexts worldwide.

6. Conclusions

The sediments deposited in the Taskourt reservoir are organized into rhythmic sequences defined by their appearance, grain size, and mineralogy. Two distinct periods have been identified as follows: the period from 2011 to 2016, during which sediment accumulation in the reservoir was particularly intense with a siltation rate of 0.77 Mm^3/year. The floods recorded in 2014 and 2016 triggered intense hydro-sedimentary dynamics resulting in a substantial sediment input. The period from 2016 to 2023 is characterized by a low sedimentation rate (0.017 Mm^3/year) due to the absence of major flood events and a prolonged drought. This trend is also reflected in the sedimentary record, with a deposit thickness limited to 32 cm.

This study demonstrates that combining bathymetric and hydrological analyses with sequential analysis of the sedimentary column provides a relevant approach for reconstructing the chronology of deposits and interpreting sedimentation processes within the reservoir. Discharge fluctuations and flood frequency emerge as key factors directly influencing the spatio-temporal variations in sedimentation rates in the Taskourt Reservoir. Extreme hydrological events within the watershed were identified using peaks-over-threshold method, with the threshold defined as the 95th percentile of the instantaneous discharge data. This approach was carried out under the assumption that the identified couplets correspond to deposits resulting from the most significant floods. The flood threshold defined as a discharge equal to or greater than 10 m^3/s provides a strong correlation between the number and thickness of couplets on one hand, and the frequency and intensity of hydrological events on the other.

This study emphasizes the vertical variation in dominant mineral phases within the reservoir sediment core, a variation that reflects both differential sedimentation processes and the fluctuations in discharge recorded in the Assif El-Mal stream. It further highlights the nature and provenance of the clays deposited in the Taskourt reservoir basin, as well as the complexity of the mechanisms governing sediment deposition in semi-arid regions. In the Assif El-Mal watershed, clay assemblages in soils are primarily detrital, inherited

from the local source rocks. The characteristics of clays accumulated in the Taskourt reservoir during a specific flood event mirror the properties of soils impacted by the associated precipitation.

The results obtained provide a transferable methodological framework that can be applied at a global scale, particularly in arid and semi-arid regions, where strong hydro-sedimentary variability exacerbates reservoir sedimentation problems. These reservoirs are essential infrastructures for mitigating the impacts of water scarcity and the irregularity of hydrological inputs.

Author Contributions: Conceptualization, M.A.; methodology, M.A., L.D., A.R. and N.F.; software, M.A.; validation, M.A., L.D., A.R. and N.F.; investigation, M.A., L.D., A.R. and N.F.; data curation, M.A., A.R. and N.F.; writing—original draft preparation, M.A.; writing—review and editing, M.A., L.D., A.R. and N.F.; supervision, L.D. All authors have read and agreed to the published version of the manuscript.

Funding: This research received no external funding.

Institutional Review Board Statement: Not applicable

Informed Consent Statement: Not applicable

Data Availability Statement: The datasets used and analyzed in the present work are available upon request to the corresponding author.

Acknowledgments: M.A. is grateful to the CNRST of Morocco (Grant PPR1/2015/63) and the "PhD-Associate Scholarship—PASS" for scholarship program. We also thank the ABHT (Tensift Water Basin Agency) and the Ministry of Equipment and Water for providing the data used in this study, including bathymetric measurements, instantaneous flow data, reservoir water volume variations, and filling rate records.

Conflicts of Interest: The authors declare no conflicts of interest.

References

1. Ekhtiari, M.; Zandieh, M.; Tirkolaee, E.B. Optimizing the Dam Site Selection Problem Considering Sustainability Indicators and Uncertainty: An Integrated Decision-Making Approach. *J. Clean. Prod.* **2023**, *428*, 139240. https://doi.org/10.1016/j.jclepro.2023.139240.
2. ICOLD World Register of Dams: General Synthesis. Available online: https://www.icold-cigb.org/GB/world_register/general_synthesis.asp (accessed on 10 June 2025).
3. Serbaji, M.M.; Bouaziz, M.; Weslati, O. Soil Water Erosion Modeling in Tunisia Using RUSLE and GIS Integrated Approaches and Geospatial Data. *Land* **2023**, *12*, 548. https://doi.org/10.3390/land12030548.
4. Gourfi, A.; Daoudi, L.; Ben Daoud, N.; Fagel, N. Clay Minerals in Soils and Sediment as Tracers of Provenance: The Case Study of the N'fis Watershed, Morocco. *Soil Use Manag.* **2024**, *40*, e12925. https://doi.org/10.1111/sum.12925.
5. Cerdà, A.; Morera, A.G.; Bodí, M.B. Soil and Water Losses from New Citrus Orchards Growing on Sloped Soils in the Western Mediterranean Basin. *Earth Surf. Process. Landf.* **2009**, *34*, 1822–1830. https://doi.org/10.1002/esp.1889.
6. Oudchaira, S.; Rhoujjati, A.; Hanich, L.; EL Hachimi, M.L. Evaluating Soil Loss and Sediment Yield for Sustainable Management of the Hassan II Dam within Morocco's Upper Moulouya Watershed Using RUSLE Model and GIS. *Environ. Earth Sci.* **2024**, *83*, 210. https://doi.org/10.1007/s12665-024-11518-0.
7. Bammou, Y.; Benzougagh, B.; Bensaid, A.; Igmoullan, B.; Al-Quraishi, A.M.F. Mapping of Current and Future Soil Erosion Risk in a Semi-Arid Context (Haouz Plain—Marrakech) Based on CMIP6 Climate Models, the Analytical Hierarchy Process (AHP) and RUSLE. *Model. Earth Syst. Environ.* **2024**, *10*, 1501–1514. https://doi.org/10.1007/s40808-023-01845-9.
8. Lamane, H.; Mouhir, L.; Zouahri, A.; Baghdad, B.; El Bilali, A.; Moussadek, R. Modeling Soil Erosion and Sediment Yield under Climate Change: A Comparison of RUSLE and MUSLE Integrated with SDR Using Variable Soil Data Resolutions. *Model. Earth Syst. Environ.* **2025**, *11*, 343. https://doi.org/10.1007/s40808-025-02544-3.

9. Bammou, Y.; Benzougagh, B.; Igmoullan, B.; Al-Quraishi, A.M.F.; Ghaib, F.A.; Kader, S. Assessing Soil Erosion Vulnerability in Semi-Arid Haouz Plain, Marrakech, Morocco: Land Cover, Socio-Spatial Mutations, and Climatic Variations. In *Natural Resources Deterioration in MENA Region: Land Degradation, Soil Erosion, and Desertification*; Springer: Berlin/Heidelberg, Germany, 2024; pp. 113–133. https://doi.org/10.1007/978-3-031-58315-5_7.
10. Mosaid, H.; Barakat, A.; Bouras, E.H.; Ismaili, M.; El Garnaoui, M.; Abdelrahman, K.; Kahal, A.Y. Dam Siltation in the Mediterranean Region Under Climate Change: A Case Study of Ahmed El Hansali Dam, Morocco. *Water* **2024**, *16*, 3108. https://doi.org/10.3390/w16213108.
11. Benzougagh, B.; Al-Quraishi, A.M.F.; Bammou, Y.; Kader, S.; El Brahimi, M.; Sadkaoui, D.; Ladel, L. Spectral Angle Mapper Approach (SAM) for Land Degradation Mapping: A Case Study of the Oued Lahdar Watershed in the Pre-Rif Region (Morocco). In *Natural Resources Deterioration in MENA Region: Land Degradation, Soil Erosion, and Desertification*; Springer: Berlin/Heidelberg, Germany, 2024; pp. 15–35. https://doi.org/10.1007/978-3-031-58315-5_2.
12. Salhi, A.; Benabdelouahab, S.; Heggy, E. Soil Erosion Susceptibility Maps and Raster Dataset for the Hydrological Basins of North Africa. *Sci. Data* **2025**, *12*, 65. https://doi.org/10.1038/s41597-025-04406-0.
13. Gourfi, A.; Daoudi, L.; Shi, Z. The Assessment of Soil Erosion Risk, Sediment Yield and Their Controlling Factors on a Large Scale: Example of Morocco. *J. Afr. Earth Sci.* **2018**, *147*, 281–299. https://doi.org/10.1016/j.jafrearsci.2018.06.028.
14. Arrebei, N.; Sabir, M.; Naimi, M.; Chikhaoui, M.; Raclot, D. Reconstitution Des Données Historiques et Diagnostic de l'état Actuel Des Aménagements Antiérosifs Dans Le Bassin Versant Nekor. *Rev. Mar. Sci. Agron. Vét.* **2019**, *7*, 267–272.
15. Lamane, H.; Moussadek, R.; Baghdad, B.; Mouhir, L.; Briak, H.; Laghlimi, M.; Zouahri, A. Soil Water Erosion Assessment in Morocco through Modeling and Fingerprinting Applications: A Review. *Heliyon* **2022**, *8*, e10209. https://doi.org/10.1016/j.heliyon.2022.e10209.
16. Romero-Díaz, A.; Alonso-Sarriá, F.; Martínez-Lloris, M. Erosion Rates Obtained from Check-Dam Sedimentation (SE Spain). A Multi-Method Comparison. *Catena* **2007**, *71*, 172–178. https://doi.org/10.1016/j.catena.2006.05.011.
17. Verstraeten, G.; Prosser, I.P. Modelling the Impact of Land-Use Change and Farm Dam Construction on Hillslope Sediment Delivery to Rivers at the Regional Scale. *Geomorphology* **2008**, *98*, 199–212. https://doi.org/10.1016/j.geomorph.2006.12.026.
18. Zhao, G.; Klik, A.; Mu, X.; Wang, F.; Gao, P.; Sun, W. Sediment Yield Estimation in a Small Watershed on the Northern Loess Plateau, China. *Geomorphology* **2015**, *241*, 343–352. https://doi.org/10.1016/j.geomorph.2015.04.020.
19. Gourfi, A.; Daoudi, L.; Rhoujjati, A.; Benkaddour, A.; Fagel, N. Use of Bathymetry and Clay Mineralogy of Reservoir Sediment to Reconstruct the Recent Changes in Sediment Yields from a Mountain Catchment in the Western High Atlas Region, Morocco. *Catena* **2020**, *191*, 104560. https://doi.org/10.1016/j.catena.2020.104560.
20. Zhao, G.; Mu, X.; Han, M.; An, Z.; Gao, P.; Sun, W.; Xu, W. Sediment Yield and Sources in Dam-Controlled Watersheds on the Northern Loess Plateau. *Catena* **2017**, *149*, 110–119. https://doi.org/10.1016/j.catena.2016.09.010.
21. Bussi, G.; Rodríguez-Lloveras, X.; Francés, F.; Benito, G.; Sánchez-Moya, Y.; Sopeña, A. Sediment Yield Model Implementation Based on Check Dam Infill Stratigraphy in a Semiarid Mediterranean Catchment. *Hydrol. Earth Syst. Sci.* **2013**, *17*, 3339–3354. https://doi.org/10.5194/hess-17-3339-2013.
22. Brignone, G.; Romero, M.; de Vries, M.V.W.; Ito, E.; Shapley, M.; Piovano, E.L. Do Ice-Dam Rupture Events Leave a Distinctive Signature in Proglacial Lake Sediments? *Quat. Res.* **2024**, *123*, 70–82. https://doi.org/10.1017/qua.2024.39.
23. Kotti, F.; Dezileau, L.; Mahé, G.; Habaieb, H.; Bentkaya, M.; Dieulin, C.; Amrouni, O. Etude de l'impact Des Barrages Sur La Réduction Des Transports Sédimentaires Jusqu'à La Mer Par Approche Paléohydrologique Dans La Basse Vallée de La Medjerda. *Proc. Int. Assoc. Hydrol. Sci.* **2018**, *377*, 67–76. https://doi.org/10.5194/piahs-377-67-2018.
24. Chalaux-Clergue, T.; Foucher, A.; Chaboche, P.A.; Hayashi, S.; Tsuji, H.; Wakiyama, Y.; Huon, S.; Vandromme, R.; Cerdan, O.; Nakao, A.; et al. Impacts of Farmland Decontamination on 137Cs Transfers in Rivers after Fukushima Nuclear Accident: Evidence from a Retrospective Sediment Core Study. *Sci. Total Environ.* **2024**, *947*, 174546. https://doi.org/10.1016/j.scitotenv.2024.174546.
25. Sabatier, P.; Moernaut, J.; Bertrand, S.; Van Daele, M.; Kremer, K.; Chaumillon, E.; Arnaud, F. A Review of Event Deposits in Lake Sediments. *Quaternary* **2022**, *5*, 34. https://doi.org/10.3390/quat5030034.
26. Wei, Y.; He, Z.; Li, Y.; Jiao, J.; Zhao, G.; Mu, X. Sediment Yield Deduction from Check–Dams Deposition in the Weathered Sandstone Watershed on the North Loess Plateau, China. *Land Degrad. Dev.* **2017**, *28*, 217–231. https://doi.org/10.1002/ldr.2628.
27. Kämpf, L.; Brauer, A.; Swierczynski, T.; Czymzik, M.; Mueller, P.; Dulski, P. Processes of Flood-Triggered Detrital Layer Deposition in the Varved Lake Mondsee Sediment Record Revealed by a Dual Calibration Approach. *J. Quat. Sci.* **2014**, *29*, 475–486. https://doi.org/10.1002/jqs.2721.

28. Salma, K.; Ahmed, A.; Abdellah, A.; Saloua, A.; Karima, I. Contribution of GIS and Remote Sensing for the Mapping, Analysis and Forecasting of Susceptible Areas to Erosion in the Assif El Mal Watershed. *Indian J. Environ. Prot.* **2023**, *43*, 41–47.
29. Weit, A.; Mourier, B.; Fretaud, T.; Winiarski, T. Combined Usage of Geophysical Methods in Continental Water Bodies, Their Benefits and Challenging Issues: A Special Focus on Sediment Deposits in Dam Reservoirs. *J. Appl. Geophys.* **2023**, *213*, 105036. https://doi.org/10.1016/j.jappgeo.2023.105036.
30. Heiri, O.; Lotter, A.F.; Lemcke, G. Loss on Ignition as a Method for Estimating Organic and Carbonate Content in Sediments: Reproducibility and Comparability of Results. *J. Paleolimnol.* **2001**, *25*, 101–110. https://doi.org/10.1023/A:1008119611481.
31. Moore, D.M.; Reynolds, R.C., Jr. *X-Ray Diffraction and the Identification and Analysis of Clay Minerals*, 2nd ed.; Oxford University Press: New York, NY, USA, 1997.
32. Cook, H.E.; Johnson, P.D.; Matti, J.C.; Zemmels, I. Methods of Sample Preparation and X-Ray Diffraction Data Analysis, X-Ray Mineralogy Laboratory, Deep Sea Drilling Project, University of California, Riverside. In *Initial Reports of the Deep Sea Drilling Project*; U.S. Government Publishing Office: Washington, DC, USA, 1975; Volume 28.
33. Moore, D.M.; Reynolds, R.C., Jr. *X-Ray Diffraction and the Identification and Analysis of Clay Minerals*; Oxford University Press: New York, NY, USA, 1989; Volume 38.
34. Fagel, N.; Boski, T.; Likhoshway, L.; Oberhaensli, H. Late Quaternary Clay Mineral Record in Central Lake Baikal (Academician Ridge, Siberia). *Palaeogeogr. Palaeoclimatol. Palaeoecol.* **2003**, *193*, 159–179. https://doi.org/10.1016/S0031-0182(02)00633-8.
35. Khalid, H.W.; Khalil, R.M.Z.; Qureshi, M.A. The Egyptian Journal of Remote Sensing and Space Sciences Evaluating Spectral Indices for Water Bodies Extraction in Western Tibetan Plateau. *Egypt. J. Remote Sens. Sp. Sci.* **2021**, *24*, 619–634. https://doi.org/10.1016/j.ejrs.2021.09.003.
36. Houmma, I.H.; Hadri, A.; Boudhar, A.; Karaoui, I.; Oussaoui, S.; El Khalki, E.M.; Chehbouni, A.; Kinnard, C. Analysis of the Propagation Characteristics of Meteorological Drought to Hydrological Drought and Their Joint Effects on Low-Flow Drought Variability in the Oum Er Rbia Watershed, Morocco. *Remote Sens.* **2025**, *17*, 281. https://doi.org/10.3390/rs17020281.
37. Benzougagh, B.; Meshram, S.G.; El Fellah, B.; Mastere, M.; Dridri, A.; Sadkaoui, D.; Mimich, K.; Khedher, K.M. Combined Use of Sentinel-2 and Landsat-8 to Monitor Water Surface Area and Evaluated Drought Risk Severity Using Google Earth Engine. *Earth Sci. Inform.* **2022**, *15*, 929–940. https://doi.org/10.1007/s12145-021-00761-9.
38. Mathewos, M.; Wosoro, D.; Wondrade, N. Quantification of Soil Erosion and Sediment Yield Using the RUSLE Model in Boyo Watershed, Central Rift Valley Basin of Ethiopia. *Heliyon* **2024**, *10*, e31246. https://doi.org/10.1016/j.heliyon.2024.e31246.
39. Alebachew, E.D.; Abiye, W.; Dengiz, O.; Turan, İ.D. Soil Erosion Estimation and Risk Assessment Based on RUSLE in Google Earth Engine (GEE) in Turkiye. *Ann. GIS* **2025**, *31*, 123–141. https://doi.org/10.1080/19475683.2025.2452262.
40. Renard, K.; Foster, G.; Weesies, G.; McCool, D.; Yoder, D. *Predicting Soil Erosion by Water: A Guide to Conservation Planning with the Revised Universal Soil Loss Equation (RUSLE)*; United States Department of Agriculture, Agricultural Research Service: Washington, DC, USA, 1997; Volume 703.
41. Wischmeier, W.H.; Smith, D.D. *Predicting Rainfall Erosion Losses: A Guide to Conservation Planning*; United States Department of Agriculture, Science and Education Administration: Washington, DC, USA, 1978.
42. Sharpley, A.N.; Williams, J.R. *Erosion/Productivity Impact Calculator: 1. Model Documentation (EPIC)*; United States Department of Agriculture, Agricultural Research Service: Washington, DC, USA, 1990.
43. Ben Daoud, N.; Daoudi, L.; Rachdane, M.; Gourfi, A.; Saidi, M.E. Suitability of Satellite-Based Rainfall Products for Estimating Rainfall Erosivity in Areas with Contrasted Climate and Terrain Properties: Example of West-Central Morocco. *J. Earth Syst. Sci.* **2024**, *133*, 78. https://doi.org/10.1007/s12040-024-02287-2.
44. van der Knijff, J.M.; Jones, R.J.A.; Montanarella, L. *Soil Erosion Risk Assessment in Europe*; EUR 19022; European Soil Bureau: Ispra, Italy, 2000.
45. Elmouden, A.; Alahiane, N.; El Faskaoui, M.; El Morjani, Z.E.A. Dams Siltation and Soil Erosion in the Souss-Massa River Basin. In *Handbook of Environmental Chemistry*; Springer: Berlin/Heidelberg, Germany, 2017; Volume 53, pp. 95–120, ISBN 9783319511290.
46. Williams, J.R.; Berndt, H.D. Sediment Yield Computed with Universal Equation. *ASCE J. Hydraul. Div.* **1972**, *98*, 2087–2098. https://doi.org/10.1061/jyceaj.0003498.
47. Boyce, R.C. Sediment Routing with Sediment Delivery Ratios. *Present Prospect. Technol. ARS/USDA* **1975**, *40*, 61.
48. Vanoni, V.A. Sediment Deposition Engineering. *ASCE Man. Rep. Eng. Pract.* **1975**, *54*, 745.
49. Rachdane, M.; Saidi, M.E.; El Khalki, E.M.; Hadri, A.; Boughdadi, S.; Nehmadou, M.; Ahbari, A.; Tramblay, Y. Unraveling Flood Dynamics at Sub-Daily Time Scales in Semi-Arid to Arid Basins in South Morocco. *Nat. Hazards* **2024**, *121*, 5413–5433. https://doi.org/10.1007/s11069-024-07022-0.

50. Farquharson, F.A.K.; Meigh, J.R.; Sutcliffe, J.V. Regional Flood Frequency Analysis in Arid and Semi-Arid Areas. *J. Hydrol.* **1992**, *138*, 487–501. https://doi.org/10.1016/0022-1694(92)90132-F.
51. Tramblay, Y.; Villarini, G.; Zhang, W. Observed Changes in Flood Hazard in Africa. *Environ. Res. Lett.* **2020**, *15*, 1040b5. https://doi.org/10.1088/1748-9326/abb90b.
52. Zhang, Q.; Gu, X.; Singh, V.P.; Xiao, M. Flood Frequency Analysis with Consideration of Hydrological Alterations: Changing Properties, Causes and Implications. *J. Hydrol.* **2014**, *519*, 803–813. https://doi.org/10.1016/j.jhydrol.2014.08.011.
53. Tramblay, Y.; El Khalki, E.M.; Khedimallah, A.; Sadaoui, M.; Benaabidate, L.; Boulmaiz, T.; Boutaghane, H.; Dakhlaoui, H.; Hanich, L.; Ludwig, W.; et al. Regional Flood Frequency Analysis in North Africa. *J. Hydrol.* **2024**, *630*, 130678. https://doi.org/10.1016/j.jhydrol.2024.130678.
54. Ben Slimane, A.; Raclot, D.; Evrard, O.; Sanaa, M.; Lefèvre, I.; Ahmadi, M.; Tounsi, M.; Rumpel, C.; Ben Mammou, A.; Le Bissonnais, Y. Fingerprinting Sediment Sources in the Outlet Reservoir of a Hilly Cultivated Catchment in Tunisia. *J. Soils Sediments* **2013**, *13*, 801–815. https://doi.org/10.1007/s11368-012-0642-6.
55. Valero-Garcés, B.L.; Navas, A.; Machín, J.; Walling, D. Sediment Sources and Siltation in Mountain Reservoirs: A Case Study from the Central Spanish Pyrenees. *Geomorphology* **1999**, *28*, 23–41. https://doi.org/10.1016/S0169-555X(98)00096-8.
56. Wang, W.; Fang, N.; Shi, Z.; Lu, X. Prevalent Sediment Source Shift after Revegetation in the Loess Plateau of China: Implications from Sediment Fingerprinting in a Small Catchment. *Land Degrad. Dev.* **2018**, *29*, 3963–3973. https://doi.org/10.1002/ldr.3144.
57. ABHT Gestion Des Phénomènes Extrêmes (Inondations). Available online: https://abht.ma/activites/gestion-des-phenomenes-extremes/inondations/ (accessed on 16 January 2025).
58. FloodList. More Heavy Rain in Morocco Prompts High Level Flood Warnings. Available online: https://floodlist.com/africa/heavy-rain-morocco-prompts-high-level-flood-warnings (accessed on 20 January 2025).
59. Rosburg, T.T.; Nelson, P.A.; Sholtes, J.S.; Bledsoe, B.P. The Effect of Flow Data Resolution on Sediment Yield Estimation and Channel Design. *J. Hydrol.* **2016**, *538*, 429–439. https://doi.org/10.1016/j.jhydrol.2016.04.040.
60. Mulder, T.; Chapron, E. Flood Deposits in Continental and Marine Environments: Character and Significance. In *Sediment Transfer from Shelf to Deep Water—Revisiting the Delivery System*; American Association of Petroleum Geologists: Tulsa, OK, USA, 2021. https://doi.org/10.1306/13271348st613436.
61. Benkirane, M.; Gourfi, A.; Millares, A.; Laftouhi, N.E.; Khabba, S. How Can Flash Flood, Snowmelt, Topography, and Land Use Changes Affect Soil Erosion and Reservoir Sedimentation in a Semi-Arid Mountainous Watershed Located in the Moroccan High Atlas? In Proceedings of the 39th IAHR World Congress, Granada, Spain, 9–24 June 2022; p. SS-1. https://doi.org/10.3850/IAHR-39WC252171192022SS368.
62. Bammou, Y.; Benzougagh, B.; Abdessalam, O.; Brahim, I.; Kader, S.; Spalevic, V.; Sestras, P.; Ercişli, S. Machine Learning Models for Gully Erosion Susceptibility Assessment in the Tensift Catchment, Haouz Plain, Morocco for Sustainable Development. *J. Afr. Earth Sci.* **2024**, *213*, 105229. https://doi.org/10.1016/j.jafrearsci.2024.105229.
63. Ouaba, M.; El Khalki, E.M.; Saidi, M.E.; Alam, M.J. Bin Estimation of Flood Discharge in Ungauged Basin Using GPM-IMERG Satellite-Based Precipitation Dataset in a Moroccan Arid Zone. *Earth Syst. Environ.* **2022**, *6*, 541–556. https://doi.org/10.1007/s41748-022-00296-z.
64. El Khalki, E.; Tramblay, Y.; Massari, C.; Brocca, L.; Simonneaux, V.; Gascoin, S.; El Mehdi Saidi, M. Challenges in Flood Modeling over Data-Scarce Regions: How to Exploit Globally Available Soil Moisture Products to Estimate Antecedent Soil Wetness Conditions in Morocco. *Nat. Hazards Earth Syst. Sci.* **2020**, *20*, 2591–2607. https://doi.org/10.5194/nhess-20-2591-2020.
65. Li, X.; Wei, X. Analysis of the Relationship between Soil Erosion Risk and Surplus Floodwater during Flood Season. *J. Hydrol. Eng.* **2014**, *19*, 1294–1311. https://doi.org/10.1061/(asce)he.1943-5584.0000912.
66. Hilgert, S.; Sotiri, K.; Fuchs, S. Review of Methods of Sediment Detection in Reservoirs. *Int. J. Sediment Res.* **2024**, *39*, 28–43. https://doi.org/10.1016/j.ijsrc.2023.12.004.
67. Chamley, H. *Clay Sedimentology*; Springer Nature: Durham, NC, USA, 1989; p. 623.
68. Omdi, F.E.; Daoudi, L.; Fagel, N. Origin and Distribution of Clay Minerals of Soils in Semi-Arid Zones: Example of Ksob Watershed (Western High Atlas, Morocco). *Appl. Clay Sci.* **2018**, *163*, 81–91. https://doi.org/10.1016/j.clay.2018.07.013.
69. Deng, Z.; Huang, D.; He, Q.; Chassagne, C. Review of the Action of Organic Matter on Mineral Sediment Flocculation. *Front. Earth Sci.* **2022**, *10*, 965919. https://doi.org/10.3389/feart.2022.965919.
70. Xue, B.; Huang, L.; Li, X.; Lu, J.; Gao, R.; Kamran, M. Effect of Clay Mineralogy and Soil Organic Carbon in Aggregates under Straw Incorporation. *Agronomy* **2022**, *12*, 534. https://doi.org/10.3390/agronomy12020534.
71. Marzougui, A.; Ben Mammou, A. Quantification et Étude Géotechnique Des Alluvions Déposées Dans La Retenue Du Barrage Joumine (Nord de La Tunisie). *Rev. Française Géotech.* **2008**,125, 29–40. https://doi.org/10.1051/geotech/2008125029.

72. Cabral, P.; Ramalho, F.L.; Gomes, S.; Rocha, H.M.; Becegato, V.A.; Paulino, A.T. Evaluation of Sediment Deposition Processes in Hydroelectric Plant: Case Study of Espora Reservoir, Brazil. *Water* **2026**, *18*, 94. https://doi.org/10.3390/w18010094.
73. Zhang, J.; Yang, M.; Zhang, F.; Tang, Y.; Wang, X.; Wang, Y. Revealing Soil Erosion Characteristics Using Deposited Sediment Sources in a Complex Small Catchment in the Wind-Water Erosion Crisscross Region of the Chinese Loess Plateau. *Geoderma* **2020**, *379*, 114634. https://doi.org/10.1016/j.geoderma.2020.114634.